



Molecular evidence of shipping noise impact on the blue mussel, a key species for the sustainability of coastal marine environments

Delphine Veillard^{1, #}, Stéphane Beauclercq^{2, #}, Nathan Ghafari², Alexandre A. Arnold², Bertrand Genard³, Lekha Sleno², Frédéric Olivier^{4, 5}, Anne Choquet⁶, Dror E. Warschawski⁷, Isabelle Marcotte², Réjean Tremblay^{1, *}

¹Institut des Sciences de la Mer de Rimouski, Université du Québec à Rimouski, Rimouski, QC G5L 3A1, Canada

²Department of Chemistry, Université du Québec à Montréal, Montréal, QC H3C 3P8, Canada

³Les Laboratoires Iso-BioKem Inc., Rimouski, QC G5L 3A1, Canada

⁴Laboratoire de 'Biologie des Organismes et Écosystèmes Aquatiques' (BOREA), Muséum national d'Histoire naturelle, Sorbonne Université, Université des Antilles, Centre National de la Recherche Scientifique, Institut de Recherche pour le Développement-207, 75005 Paris, France

⁵Université Bretagne Occidentale (UBO), CNRS, IRD, Institut Universitaire Européen de la Mer, Plouzané, France

⁶Univ Brest, Ifremer, CNRS, UMR 6308, AMURE, IUEM, 29280 Plouzané, France

⁷Chimie Physique et Chimie du Vivant, CPCV, CNRS UMR 8228, Sorbonne Université, École normale supérieure, PSL University, 75005 Paris, France

ABSTRACT: Global anthropogenic oceanic noise caused by shipping is predicted to double every 11.5 yr, putting marine organisms at risk. While the impact of noise on marine mammals is well documented, its effects on molluscs, which hold immense economic and ecological importance, remain largely unknown. To investigate the consequences of noise on mollusc metabolism during crucial early life stages, blue mussel *Mytilus edulis* larvae were exposed to shipping noise in a laboratory setting until the post-larval stage and their metabolome was analysed. Multivariate analyses of the metabolome showed that shipping noise induced stress-related inflammation with increased energy demand, higher protein turnover, and disrupted nervous system activity. Consequently, noise promoted delayed metamorphosis in suboptimal habitats with greater metabolic costs, which may affect ecosystem and aquaculture sustainability as competent mussel larvae struggle to select suitable development habitats. Without action to limit underwater noise, such impacts could disrupt population structures and marine biodiversity.

KEY WORDS: Noise pollution · *Mytilus edulis* · Post-larvae · Metabolism · Metabolomics

1. INTRODUCTION

Over the last 50 yr, shipping noise has increased the ocean ambient noise in the Northeast Pacific by 3–12 decibels referenced to a pressure of 1 microPascal (dB re 1 μ Pa) and may double globally every 11.5 yr, essentially caused by the rising number of commercial vessels (Andrew et al. 2002, McDonald et al. 2006, Frisk 2012, Jalkanen et al. 2022). In 2017, during the Conference of the Parties of the Convention on the

Conservation of Migratory Species (United Nations) (Conference of the Parties of the Convention on Migratory Species 2017), anthropogenic marine noise — primarily associated with shipping (90%) — was recognized as an emerging and poorly understood source of pollution, representing 'a potential threat to marine species conservation and welfare' (Chauvaud et al. 2018, p. 89). Ships generate low frequency noise (5–500 up to 10 000 Hz) that can reach 190 dB re 1 μ Pa at 1 m and propagate over long dis-

*Corresponding author: rejean_tremblay@uqar.ca

#These authors contributed equally to this work

tances, affecting marine organisms in various ways ranging from physical damage to masking relevant biological signals (Hawkins & Popper 2017, Duarte et al. 2021). For decades, there has been strong evidence of the negative impacts of noise on marine mammals and fish, both of which possess important auditory senses. These include behavioural, habitat, and physiological changes leading to an increase in mortality in the most extreme cases (Duarte et al. 2021). The effects on molluscs are still mostly unknown despite studies showing their ability to produce and perceive sounds through their statocysts (balance sensory receptors) and abdominal sense organs (Solé et al. 2023).

Molluscs represent 23% of the biological diversity in oceans, and among them, bivalves are especially known to be key species for the development, functioning, and sustainability of coastal environments (Smaal et al. 2019). Exposure of molluscs to anthropogenic noise could have a dramatic impact on the entire marine ecosystem and therefore must be assessed. The auditory sensing range of adult molluscs is not fully known; adult blue mussels *Mytilus edulis* have been shown to respond by valve closure to noise between 5 and 410 Hz (Roberts et al. 2015, Chauvaud et al. 2018). Anthropogenic noise effects on bivalves include changes in oxygen consumption (Wale et al. 2019), increased biochemical stress (Vazzana et al. 2016), metabolism adjustment (Peng et al. 2016), reduced growth and development (de Soto et al. 2013), modification of the recruitment process (Jolivet et al. 2016, Cervello et al. 2023), and even increased mortality (Day et al. 2017). From a behavioural perspective, anthropogenic noise could disrupt feeding and feeding rate (Spiga et al. 2016) due to a reduction in valve gape opening (Day et al. 2017, Ledoux et al. 2023). However, very few data are available on early life or larval stages of bivalves, which may be more sensitive (Rayssac et al. 2010) and are critical stages, as pediveliger larvae use environmental stimuli to settle in an optimal habitat and undergo metamorphosis (Hadfield & Paul 2001, Lillis et al. 2013, Jolivet et al. 2016, Schmidlin et al. 2024). If settlement conditions are unsuitable, pediveliger larvae can prolong their pelagic dispersal life and delay their metamorphosis for several weeks (Pechenik 1990, Martel et al. 2014). Moreover, anthropogenic sound, like vessel noise, increases mussel settlement (Wilkins et al. 2012, Jolivet et al. 2016). Metamorphosis represents a pivotal life-changing event for numerous molluscan species, marking the transition of free-swimming pelagic larvae to attached (sessile) benthic post-larvae (Joyce & Vogeler 2018). At the pediveliger stage, mussel larvae attain 'metamorphic com-

petence', initiating their transformative process with irreversible morphological and physiological changes (Hadfield 2000). These changes include the development of a foot-like structure, loss of the velum, gill development, and secretion of the juvenile shell. This metamorphic transition relies heavily on environmental cues to guide the larvae in selecting an optimal habitat for settlement and subsequent development (Hadfield & Paul 2001) (Fig. 1).

Among bivalves, the blue mussel holds immense economic and ecological importance, with worldwide aquaculture production surpassing wild catches, reaching almost 170 000 t annually, for a revenue exceeding US \$300 million (FAO 2019). Mussel farming is a source of sustainable proteins and omega-3 fatty acids. Additionally, it plays a crucial role in ecology by promoting biodiversity. Indeed, *Mytilus* is a filter-feeding organism that limits eutrophication by consuming microalgae, which enhances illuminance on benthic algae and increases the production of other benthic organisms (Borthagaray & Carranza 2007). The sessility and coastal lifestyle of mussels particularly exposes them to repeated or long-lasting anthropogenic noise. Indeed, their habitat often colocalizes with zones of intense ship traffic, as is the case in the Gulf of St. Lawrence, where 98% of Canadian mussels are produced. Canada is the top producer in the Americas and third-largest worldwide (Statistics Canada 2019). With up to 60 000 ships traversing the Gulf on a monthly basis (Pelo & Wootton 2004), effective management and prevention strategies are imperative.

The United Nations Convention on the Law of the Sea of 1982 establishes a general obligation for member states to protect and preserve the marine environment (Article 192, United Nations 1982). To address noise pollution from ships, both national and international legal frameworks are evolving. The European Union's Marine Strategy Framework Directive, specifically Descriptor 11, aims to prevent adverse effects of energy introduction, including underwater noise (Directive 2008/56/EC, European Union 2008). The International Maritime Organization (IMO) has also taken steps; in 2023, the Marine Environment Protection Committee approved revised guidelines for reducing underwater radiated noise from shipping, effective from 1 October 2023 (IMO 2023). These guidelines build upon previous ones and encourage member states to apply them in collaboration with relevant stakeholders. However, thresholds specifying the acceptability of sound levels are lacking for the enforcement of those guidelines.

In this study, the response of mussel larvae to cargo-ship sounds at different intensities recorded in

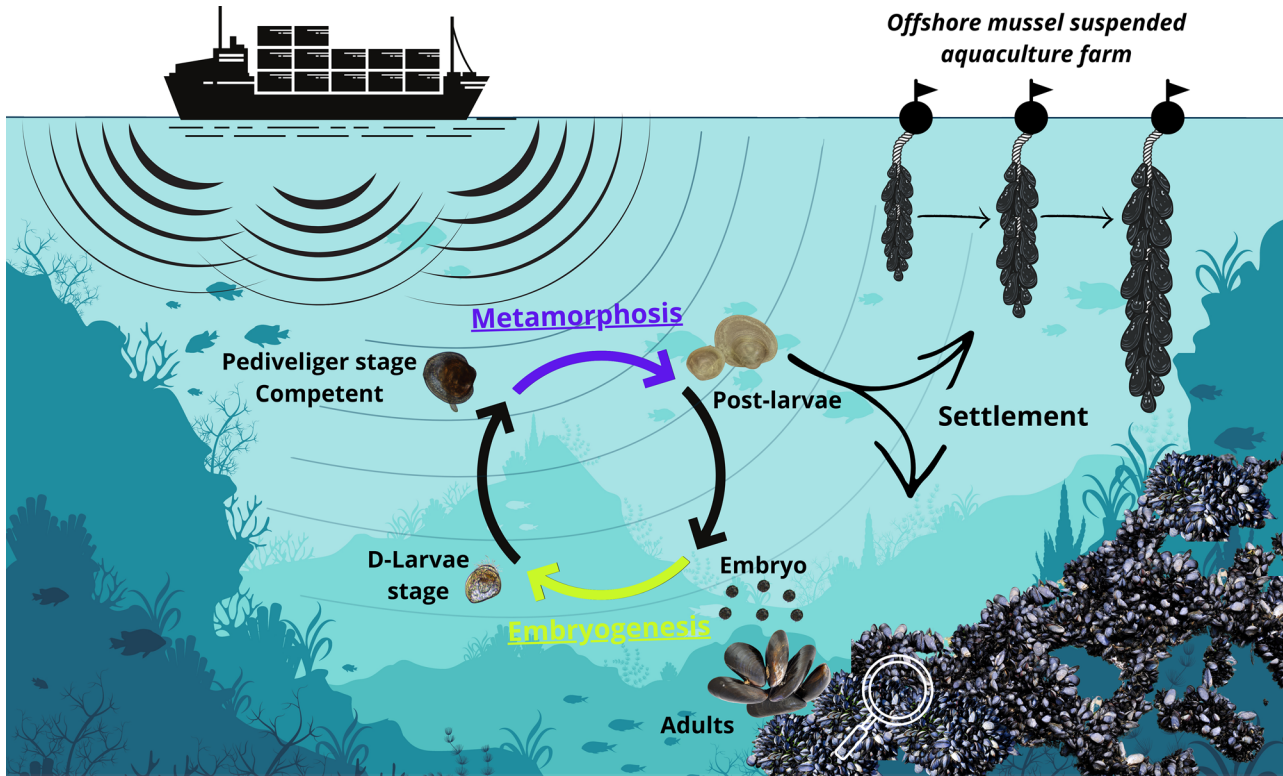


Fig. 1. Blue mussels *Mytilus edulis* exhibit a benthic-pelagic life cycle, which includes two endotrophic stages: embryogenesis and metamorphosis. These stages rely on energy reserves accumulated during the previous phase and are generally recognized as being particularly sensitive to environmental stressors. The transition through metamorphosis is strongly dependent on environmental cues, which help guide the larvae in selecting a suitable substrate for settlement — whether on aquaculture systems or in natural habitats (indicated by the magnifying glass). However, these critical cues can be disrupted by shipping noise, potentially impairing successful development and settlement

the Gulf of St. Lawrence was evaluated. To achieve this, acoustic perturbations were applied during larval metamorphosis and the subsequent stress on the post-larval metabolome, i.e. the ensemble of all of the small molecules found in an organism, was examined along 3 axes. The first axis focused on lipid mediators, such as prostaglandins and oxylipins. These molecules are responsible for processes such as inflammation (Lee et al. 2021). A targeted lipidomics approach was used to analyze them. This approach screened for 11 prostaglandins and 38 oxylipins. These oxylipins were derived from eicosapentaenoic, α/γ -linolenic, arachidonic, linoleic, and docosahexaenoic acids. The analysis was performed using liquid chromatography coupled to high-resolution tandem mass spectrometry (LC-HRMS/MS). Secondly, the polar metabolites involved in general metabolism (mainly organic acids, nucleosides, and nucleotides) were characterized by a combination of untargeted nuclear magnetic resonance (NMR) spectroscopy and LC-HRMS/MS-based metabolomics. This approach was enriched by an extensive targeted study of the amino

acid (21 compounds) and energy (27 compounds) metabolisms by LC-HRMS/MS. Finally, the third axis studied the changes in larval performance and behaviour in relation to metabolism alterations, considering that noise is a possible cue for larval settlement. This combined approach based on complementary analytical methods provides new insights into the metabolic pathways affected by this emerging pollutant in bivalves and its implications for ecosystems and mussel aquaculture sustainability.

2. MATERIALS AND METHODS

2.1. Shipping noise sampling

Noise from the 'Nohlan Ava', a 120 m long roll-on/roll-off cargo ship built in 2000, which had the most intense and distinguishable noise fingerprint in the harbour of St-Pierre-et-Miquelon (France), was recorded between November 2020 and April 2021 using an Aural-M2 (Multi-Electronique) underwater acous-

tic recorder (sampling frequency of 32 kHz, 16-bit resolution) equipped with an HTI-96-MIN hydrophone (High Tech) with a sensitivity of -165 dB re $V \mu Pa^{-1}$ and set with a gain of 22 dB. The sampling frequency (32 kHz) allowed us to capture the entire acoustic signature of the vessel as the maximum of energy is below 10 kHz. The sound sequence was selected with Audacity® software to create an 80 min soundtrack composed of the sound of the cargo ship arrival (11 min), a 39 min break (simulating handling in the harbour), its departure (8.5 min), and a new break of 21.5 min (doi:10.5281/zenodo.10910123). The loudest vessel in the archipelago of St-Pierre-et-Miquelon was selected and looped to standardize exposure to anthropogenic noise, as this approach avoided the complexities of replicating the variable acoustic landscape (e.g. day–night cycles, weekly recreational peaks, and weather-driven fluctuations). The equivalent sound levels, expressed in sound pressure level (total root mean square sound pressure level), are detailed in Table S1 in the Supplement at www.int-res.com/articles/suppl/m759p035_supp.pdf.

2.2. Mussel larval culture and sound exposure

Rearing of blue mussel larvae was performed as described by Rayssac et al. (2010) (Fig. 2). Briefly, adult mussels (50 mm shell length) from St. Peters Bay in Prince Edward Island, Canada (46.4295° N, 62.6603° W), were individually induced to spawn by 10°C thermal

shock. A ratio of 10 spermatozooids per egg was used for the fertilization in UV ultra-filtered ($1 \mu m$) seawater at 18°C. Eggs were further washed with UV ultra-filtered seawater and maintained at 18°C. The obtained embryos were divided into 6 tanks of 60 l at a density of 5 larvae ml^{-1} maintained at 18°C until over 50% of the population was at the pediveliger stage (competent larvae) at 17 d post-fertilization (dpf), i.e. eyed larvae, foot development and substrate exploration. The 6 batches were then randomly distributed among 24 cylinders of 5 l in 4 Larvosonic mesocosm tanks. Larvosonic is an innovative tank system composed of 6 circular culture cylinders of 5 l (unit of replication, with 25 000 larvae in each cylinder) designed for the exposure of organisms to sounds while limiting classical reverberation and resonance problems (Cervello et al. 2023, Olivier et al. 2023). Temperature (mean \pm SD, $18.1 \pm 0.1^\circ C$), salinity (60.8 ± 0.4 PSU), photoperiod (15:9 h of light:dark) and light intensity (97.1 ± 1.7 lx) were monitored during the experiments. During rearing and noise exposure experiments, larvae were fed every 2 d with 60 cells μl^{-1} of a mixed suspension of microalgae containing *Pavlova lutheri* (CCMP459), *Tisochrysis lutea* (CCMP1324), *Chaetoceros muelleri* (CCMP1317), *Tetraselmis suecica* (CCMP904), and *Nannochloropsis oculata* (CCMP525) at a ratio of 1:1:1:1:1 equivalent biomass (dry weight). Collectors (made from 2 polypropylene ropes, each 30 cm long) were introduced into the cylinders to allow the settlement of the larvae prior to the exposure to the recorded shipping sound. During the metamorphosis stage, pediveliger (17 dpf)

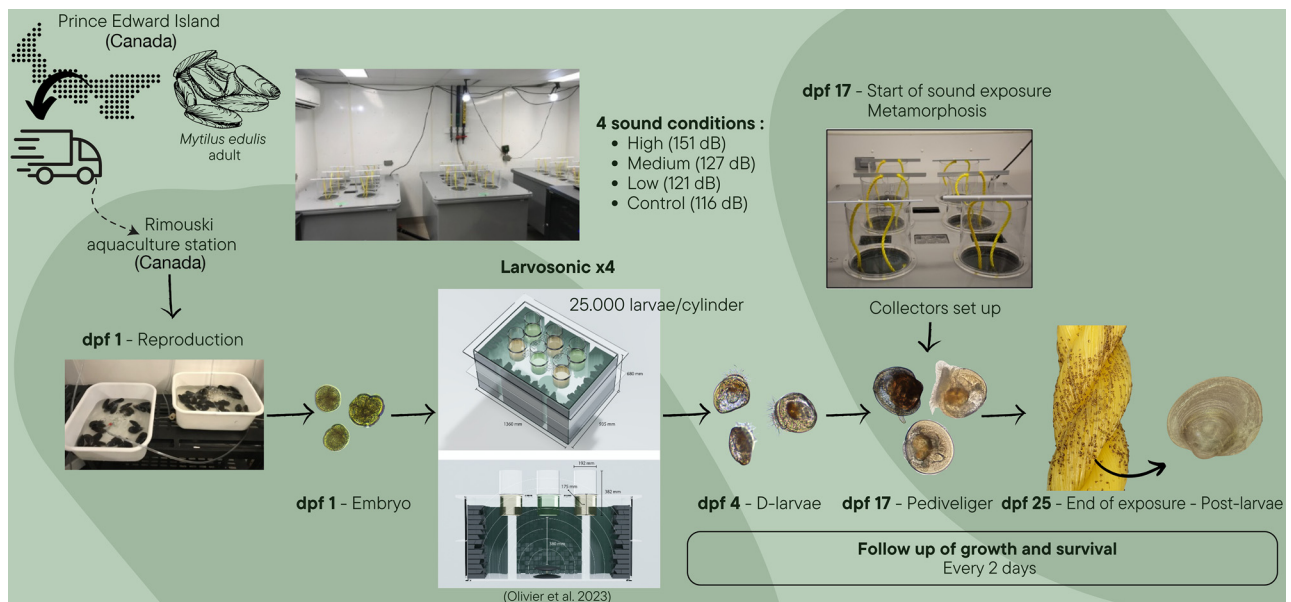


Fig. 2. Experimental procedure developed for the exposure of blue mussel larvae during metamorphosis to shipping noise. dpf: day post-fertilization

to post-larvae (25 dpf) were exposed in each Larvasonic tank to a different sound treatment for 9 d (Fig. 2): low (121 ± 4 dB re 1 μ Pa), medium (127 ± 2 dB re 1 μ Pa), high (151 ± 2 dB re 1 μ Pa), and silence playback with ambient room noise (control; 116 ± 1 dB re 1 μ Pa) (Table S1). These sound levels are the maximum emission level and are related to distance from the source (cargo ship), with a greater sound intensity closer to the source and vice versa, thus corresponding to 18.5 m (high sound exposure), 735 m (medium), and 1.8 km (low) from the source and compared to ambient lab conditions (control). These distances were calculated according to the sound propagation loss (also called transmission loss) formula taking the base of $15\log_{10}$ (Fig. S1). Every 2 d, collectors were carefully removed from each cylinder, hung up in the air to avoid juvenile detachment, and the cylinders were cleaned with Virkon VKS10 disinfectant (LANXESS Deutschland) before water changing with UV-ultrafiltered seawater and monitoring of the larval health, growth, and survival rate by optical microscopy.

At the end of the sound exposure experiment, collectors were gently rinsed with sprayers on a 100 μ m mesh sieve to retrieve post-larvae from the 24 cylinders (6 replicates per sound treatment). Settled growing post-larvae on the cylinder walls were carefully brushed off and pooled with the post-larvae from the collectors to estimate the total wet biomass of recruits. Immediately after collection, larval pools were split into 3 sub-samples, i.e. 1 for targeted metabolomics and 2 for untargeted metabolomics experiments (if the quantity of recovered post-larvae allowed it), flash-frozen in liquid nitrogen, freeze-dried, and stored at -80°C until extraction for metabolomics.

2.3. Growth and metamorphosis success

Larval growth was measured throughout the experiment using a Keyence VHX-2000 Series digital microscope with VH-Z100UR objectives (1 μ m resolution and high dynamic range imaging). The size at metamorphosis was determined by the larval shell (prodissoconch II, PII) morphology and morphometry (Bayne 1965, Martel et al. 1995). Furthermore, the metamorphosis success was calculated by the ratio of total biomass of post-larvae recovered from the collectors over the number of initial larvae put in each cylinder and the larval growth after metamorphosis by the measure of the larval shell (dissoconch, D) on post-larvae (Martel et al. 2014).

2.4. Untargeted metabolomics

The freeze-dried post-larvae pools (~ 3.4 mg or ~ 500 post-larvae) were crushed with a micro-pestle in microtubes before metabolite extraction using an adaptation of Folch's method (1 methanol:1 chloroform:1.4 water) including a 10 min sonication on ice. Extracts were centrifuged at $10\,000 \times g$ (10 min at 4°C) to separate the polar fraction. The extractions were repeated 3 more times and the polar extracts were pooled before solvent evaporation in a SpeedVac (Thermo Fisher Scientific) at room temperature.

2.4.1. Proton nuclear magnetic resonance ($^1\text{H-NMR}$)

The larval extracts were reconstituted in 500 μ l of NMR buffer (0.2 M pH 7.4 potassium phosphate buffer in 99.9% deuterium oxide with 0.13 mM 3-trimethylsilylpropionic acid) and transferred to standard 5 mm NMR tubes. The $^1\text{H-NMR}$ spectra from the post-larvae were obtained with a Bruker Avance III spectrometer, operating at 600 MHz, with a double-resonance broad-band fluorine observation probe. The spectra were further processed, binned, and integrated using NMRProcFlow tools (Jacob et al. 2017) and the identification of the metabolites was performed using Chemomx software and was further confirmed by 2D $^1\text{H-NMR}$ correlation spectroscopy and total correlation spectroscopy experiments.

2.4.2. Liquid chromatography with high-resolution tandem mass spectrometry (LC-HRMS/MS)

After NMR acquisition, the samples were recovered and analysed by LC-HRMS/MS using a Shimadzu Nexera ultra high performance liquid chromatography coupled to a quadrupole time-of-flight system (TripleTOF[®] 5600⁺, Sciex), equipped with a DuoSpray ion source operated in positive and negative electrospray mode. Metabolite separation was conducted on a mixed-mode reverse-phase column using gradient elution with mobile phases of water and acetonitrile (ACN), both containing 0.1% formic acid. Feature annotation for putative metabolite identifications was performed using MS/MS spectral matching with the NIST2017 MS/MS spectral library, Sciex 'All in one' accurate mass metabolite library, and an in-house spectral library from standard metabolites run under identical MS/MS conditions. Features with a library score ≥ 85 and an accurate mass measurement for protonated or deprotonated

precursors <10 ppm were kept for further processing. Peak integration was verified for each putatively identified metabolite using Sciex OS-Q.

More details about the $^1\text{H-NMR}$ and LC-HRMS/MS-based untargeted metabolomic experiments are provided in Texts S1.1 and S1.2. in the Supplement.

2.5. Quantification of amino acids, energy metabolism-related metabolites, and polyunsaturated fatty acid oxidation products

Around 3.5 mg of freeze-dried post-larvae (~500 post-larvae) were micro-ground and homogenized with a 2.8 mm ceramic bead at 4000 rpm for 3 cycles of 10 s (Precellys 24; Bertin). Analyte extraction for the quantification of amino acids, energy metabolism-related metabolites, and oxylipins were performed on the same sample with an extraction process in 2 steps.

The first step allows extracting the oxylipins. One millilitre of a 5:1 (v:v) mix of methyl tert-butyl ether (MTBE) and 2,2,2-trifluoroethanol (TFE) was added to the homogenizing tubes containing the sample. The samples were vortexed for 30 s and centrifuged for 1 min at $2460 \times g$. This extraction was performed 3 times, and supernatants (750 μl) were pooled in 15 ml Falcon tubes. For the second and third extraction cycles, 750 μl of 5:1 (v:v) MTBE:TFE were added to the samples. The supernatant was washed 3 times with 250 μl of LC-MS grade water. The aqueous layer was collected and pooled with supernatant obtained during the second step of the extraction protocol. The organic phase was dried using a vacuum concentrator (SpeedVac, Savant SPD2010, Thermo Fisher Scientific) for 2 h without heating. Dried samples were reconstituted with 250 μl of a 1:1:1:1 (v:v:v:v) mix of TFE:ACN:methanol:50 mM ammonium formate at pH 3. The samples were vortexed for 30 s and centrifuged for 1 min at $2460 \times g$. Then 250 μl of the supernatant were transferred to a 2 ml HPLC vial containing 1 ml of 50 mM ammonium formate buffer at pH 3 with 10 ng ml^{-1} of internal standard PGE₂-d₉. The sample was analysed directly after the extraction process.

During the second step, amino acids and energy metabolism-related metabolites were extracted. One millilitre of a 1:1 (v:v) mix of TFE:LC-MS-grade water was added to the homogenizing tubes, vortexed for 30 s and centrifuged for 1 min at $2460 \times g$. Three extraction cycles were performed, and supernatants (750 μl , except for the third extraction, in which 1 ml was used) were pooled in a 15 ml Falcon tube, containing the aqueous layer obtained during oxylipin extraction and 4 ml of ACN. For the second and third

extraction cycle, 750 μl of 1:1 (v:v) TFE:LC-MS-grade water were added to the samples. The sample was dried with a SpeedVac overnight without heating. The sample reconstitution was performed by adding 50 μl of LC-MS-grade water followed by addition of 200 μl of LC-MS-grade ACN. Aliquots (100 μl) of each reconstituted sample were transferred to 2 vials: one for the positive analysis and the other for the negative analysis. The compounds valine-d₈ (0.1 $\mu\text{g ml}^{-1}$) and pyruvate-d₃ (1 $\mu\text{g ml}^{-1}$) were used as internal standards to quantify the compounds in positive and negative ion modes, respectively.

Oxylipin analysis was performed with an HPLC 1260 Infinity II device coupled to a 6546 QTOF (Agilent Technologies) in negative ionization mode equipped with an Agilent 1290 Infinity Flexible Cube. Oxylipin extracts were separated using an InfinityLab Poroshell HPH C-18, 2.1 mm internal diameter [i.d.] \times 100 mm length, 1.9 μm particle size (Agilent) and a Gemini C6-Phenyl guard column as on-line solid-phase extraction (4 \times 2.0 mm, SecurityGuard, Phenomenex) with a column temperature maintained at 40°C.

Metabolites were separated and quantified in multiple reaction monitoring mode using an HPLC 1260 Infinity II device coupled to a 6420 Triple Quad mass spectrometer (Agilent Technologies) in positive and negative ionization mode. Ten microliters of the sample were injected, and the chromatography separation was performed with an InfinityLab Poroshell 120 HILIC-Z column (2.1 mm i.d. \times 100 mm length, 2.7 μm particle size).

Data were processed with MassHunter Quantitative QQQ (Quant-my-Way) software from Agilent Technologies. Two samples in the oxylipin analysis had bad peak shapes and a large change in retention time. These 2 samples were removed from the analysis. More details about the targeted experiments are provided in Text S1.3 in the Supplement.

2.6. Statistical analyses

2.6.1. Multivariate statistics

The metabolomics data were analysed by orthogonal projection latent structures discriminant analyses (OPLS-DA) using SIMCA 17 software (Sartorius). All data were scaled to units of variance. The minimum number of features needed for optimal classification of the control and high-noise samples in the OPLS-DA models was determined by iteratively excluding the variables with low regression coefficients and wide confidence intervals derived from

'jack-knifing' combined with low variable importance in the projection (VIP) until maximum improvement of the quality of the models. The model quality was evaluated after 7-fold cross validation by cumulative R^2Y (goodness of fit), cumulative Q^2 (goodness of prediction), CV-ANOVA (test of cross-validated predictive residuals), and by fitting principal component analyses (PCAs) which are an indicator of OPLS-DA model reliability (Eriksson et al. 2008). The contribution of each predictor in the model was evaluated through the variable score contribution, i.e. the differences, in scaled units, for all of the terms in the model, between the outlying and the normal observation, multiplied by the absolute value of the normalized weight. Metabolites included in the model with a $VIP > 1$ were considered as important. The effect of the intermediate noise levels (low and medium) on the larval metabolome was predicted from the OPLS-DA models adjusted for the control and high conditions.

To identify the most relevant metabolites across the untargeted data sets (1H -NMR, LC-HRMS/MS), an alternative model was fitted by multiblock OPLS-DA applied and structured in 2 blocks. In practice, a different block was assigned to the variables of each data set, and each block was scaled to avoid the domination of one block over the others. Thereafter, OPLS-DA was performed on the 2 blocks iteratively, excluding the least relevant variables from the model as described above.

The sets of features included in the OPLS-DA were further tested for their ability to explain the variations related to noise when modelled using PCA, an unsupervised multivariate method (Fig. S2) (Worley & Powers 2016).

2.6.2. Metabolite enrichment analysis

To identify the most significantly affected metabolic pathways, the discriminant metabolites (untargeted multiblock OPLS-DA and targeted OPLS-DA amino acid and energy metabolism) were analysed by metabolite-set enrichment analysis (Xia & Wishart 2010), implemented in Metaboanalyst, a freely available web-based metabolomics analysis suite (MetaboAnalyst 5.0, www.metaboanalyst.ca) (Pang et al. 2021). The metabolite enrichment analysis of each set of metabolites was performed using over-representation analysis with the 'pathway-associated metabolite sets' provided, containing 99 metabolite sets based on normal human metabolic pathways. The over-representation analysis was implemented using the hypergeometric test to evaluate whether a particular metabolite set was more highly

represented than expected by chance within the given compound list. A cutoff was chosen at a p-value controlled for a false discovery rate (FDR) of 0.01 to retain the most significantly enriched metabolic pathways.

2.6.3. Permutational multivariate analysis of variance (PERMANOVA)

The growth and metamorphosis success data were analysed with PRIMER7 software, using ANOVAs with 9999 permutations of residuals under a reduced model (PERMANOVA). The permutational method involves a randomization which allows us to remove the distributional assumptions such as normality and can be applied to very small samples. Similarity matrices based on ratios were produced using the Bray-Curtis distance. A 1-way PERMANOVA tested the effect of sound levels (control, low, medium, and high) on growth (size at metamorphosis and growth post-metamorphosis) and metamorphosis success. When differences were significant ($p\text{-perm} \leq 0.05$), multiple comparison pairwise tests were used to determine which groups significantly differed. Distance-based tests for homogeneity of multivariate dispersions (PERMDISP) were carried out to evaluate the homogeneity of ratios in each condition.

3. RESULTS

Spectrograms (Fig. 3a,b) highlighted sustained low-frequency energy during arrival of the 'Nohlan Ava', a 120 m roll-on/roll-off cargo ship, while energy diminished more rapidly during departure. Power spectral density (PSD) analysis of noise from the ship revealed distinct acoustic profiles during its arrival (11 min) and departure (8.5 min) phases (Fig. 3c,d). The ship's noise exhibited slightly higher energy across most frequencies during arrival. The departure phase showed reduced and more uniform sound intensity. PSD comparisons across exposure conditions (high, medium, low, and control) demonstrated significantly elevated sound intensities in high-exposure conditions (Fig. 3c,d), with medium and low exposures showing intermediate levels, and the control the lowest.

3.1. Post-larval prostaglandins and fatty acid oxidation products

The stress induced by the noise treatment could promote the oxidation of polyunsaturated fatty acids

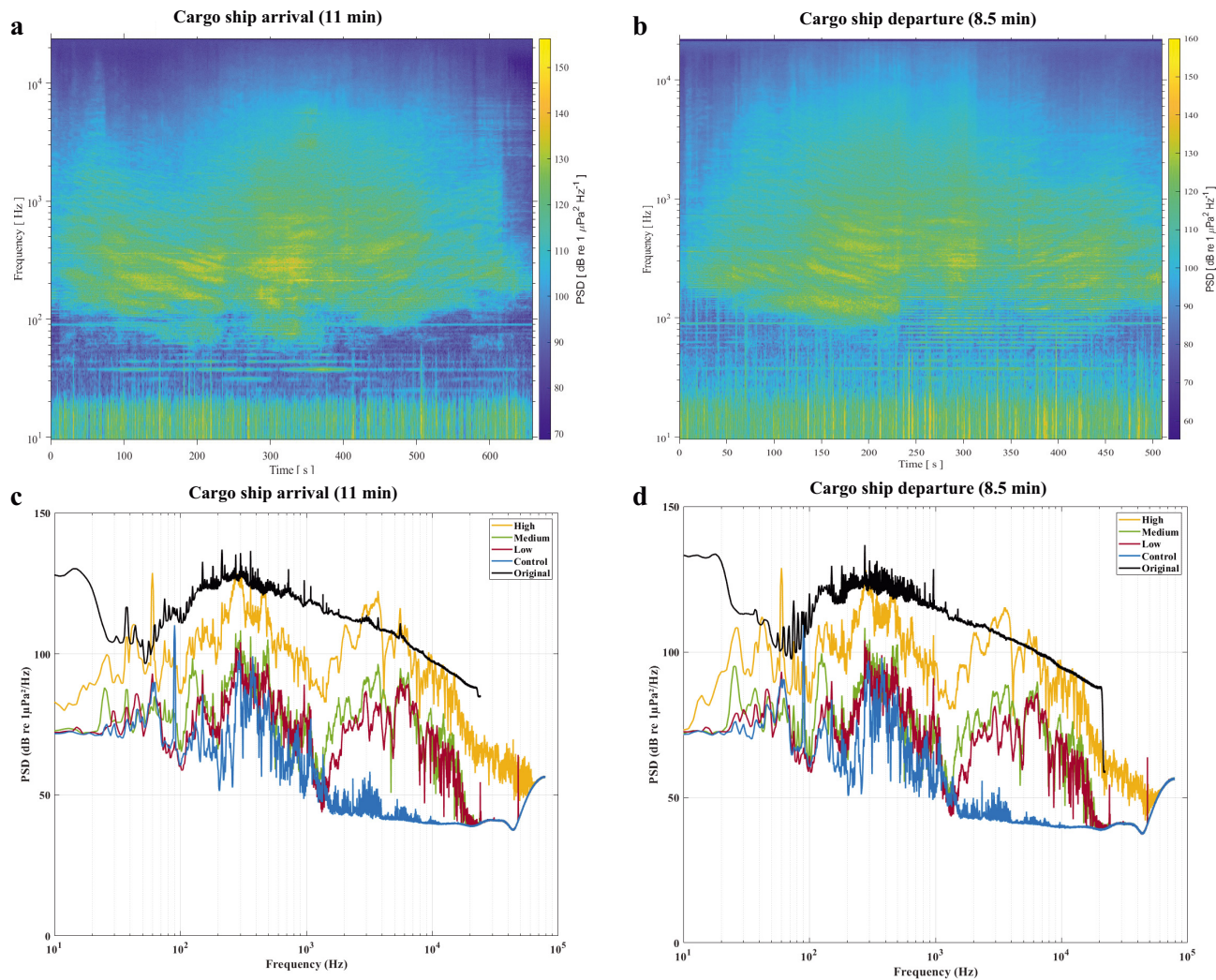


Fig. 3. Spectrograms of the cargo ship *in situ* sound during its (a) arrival and (b) departure. Power spectral density (PSD) analysis of the cargo ship original sound recorded *in situ* and at the center of the middle cylinder below the water surface, for all experimental conditions and the control, during (c) arrival and (d) departure (window length: 1 second, window type: Hann)

(PUFAs) from phospholipids notably involved in inflammatory processes. Accordingly, the cyclopentenone prostaglandins (cyPGs) derived from arachidonic acid, as well as oxylipins were quantified in blue mussel post-larvae (Table S2). An OPLS-DA (Fig. 4; Table S3) was fitted to identify the compounds from the oxidative metabolism that were differentially regulated between ambient (control, $n = 5$) and high noise (~ 151 dB re $1 \mu\text{Pa}$, $n = 5$) exposure. This model ($R^2Y = 0.97$, $Q^2 = 0.95$, CV-ANOVA = 0.0016), composed of 1 predictive and 1 orthogonal component, was able to explain the variability induced by the sound treatment (Fig. 4a) and contained 14 compounds (Fig. 4b). The larval pools exposed to low noise (~ 121 dB re $1 \mu\text{Pa}$, $n = 6$) were also correctly discriminated from those from the high sound treatment. The intermediate level (~ 127 dB re $1 \mu\text{Pa}$,

$n = 5$) induced a similar response to the high sound treatment.

As shown in Fig. 4, the OPLS-DA revealed that 5 classes of lipid mediators were affected by noise, namely (1) cyPGs; (2) omega-3 eicosapentaenoic acid-derived oxylipin; (3) α -linolenic acid-derived oxylipin; (4) linoleic acid-derived oxylipin; and (5) hydroxy docosahexaenoic acids (HDHAs). CyPGs are derived from C20-unsaturated FAs with a cyclopentane ring, formed from arachidonic acid (C20:4 ω -6) or eicosatetraenoic acid (C20:4 ω -3) through cyclooxygenation. They are rapidly metabolized by enzymatic reactions to inactive forms. The OPLS-DA showed the presence of 2 active cyPGs, i.e. PGA2, which was more concentrated in mussels exposed to noise, possibly indicating inflammation or oxidative stress (Lee et al. 2010), and PGF3 α , which was more prominent in

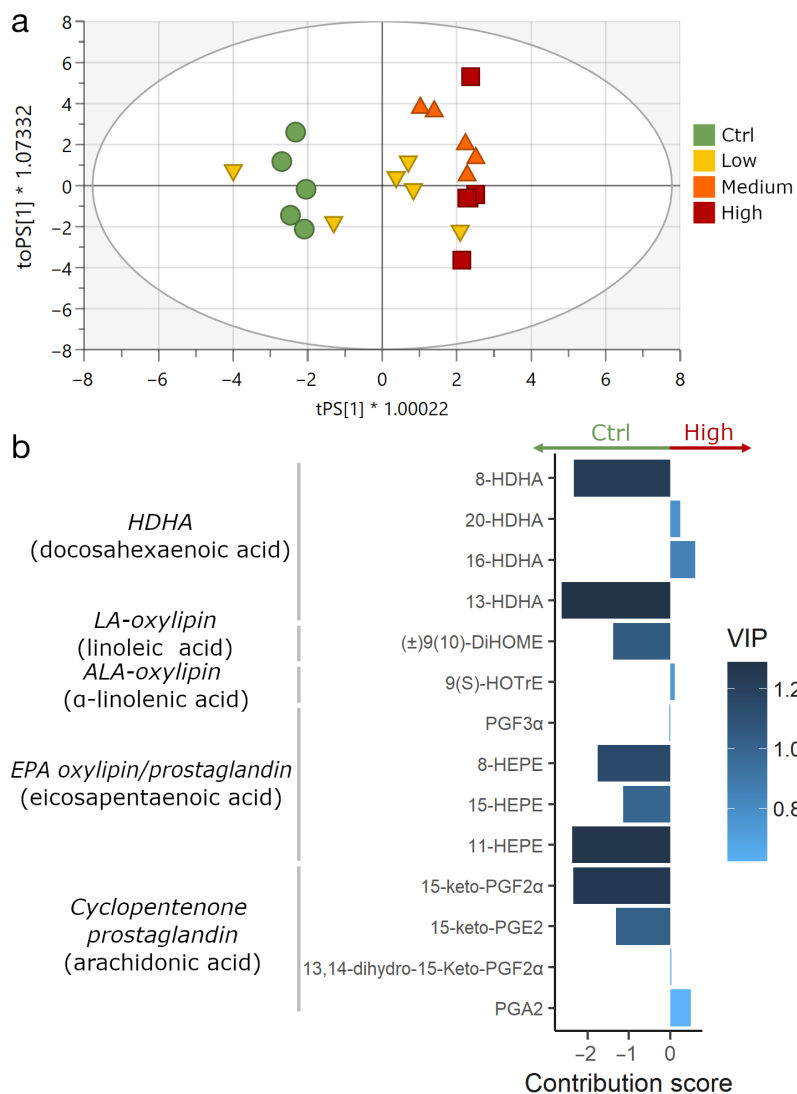


Fig. 4. Impact of shipping noise on prostaglandins and fatty acid oxidative metabolism in blue mussel post-larvae. (a) Orthogonal projection latent structures discriminant analyses (OPLS-DA) scores based on the fitted model ($R^2Y = 0.97$, $Q^2 = 0.95$, CV-ANOVA = 0.0016) of targeted lipid oxidation products quantified as a function of shipping noise level. Shipping noise treatment groups are control (Ctrl; ambient noise, $n = 5$), low (~ 121 re $1 \mu\text{Pa}$, $n = 6$), medium (~ 127 re $1 \mu\text{Pa}$, $n = 5$), and high (~ 151 dB re $1 \mu\text{Pa}$, $n = 5$). (b) Contribution and importance in the model (variable importance in the projection, VIP) of the compounds identified by the OPLS-DA-based screening to explain the impact of shipping noise on the post-larval mussel metabolome

control samples. Inactivated prostaglandins 15-keto-PGF 2α and 13,14-dihydro-15-keto-PGF 2α were also detected in mussel larvae exposed to medium and high noise levels. The inactivation products of PGE 2 , i.e. 15-keto-PGE 2 and 15-deoxy- $\Delta 12,14$ -prostaglandin J 2 , were more concentrated in the controls, indicating the termination of proinflammatory reactions (Kim et al. 2021). Oxylipins — resulting from the oxidation of eicosapentaenoic acid (C $20:5 \omega$ -3), i.e.

α -linolenic acid (C $18:3\omega$ -3) and linoleic acid (C $18:2\omega$ -6) — were generally higher in controls. Finally, 4 HDHAs, which derive from docosahexaenoic acid (C $22:6\omega$ -3), were retained in the OPLS-DA.

3.2. Post-larval polar metabolites

The response to stress could also impact general metabolism, such as amino acid synthesis or catabolism in relation with energy metabolism, and the synthesis/degradation of DNA and RNA, and could involve multiple classes of molecules. Therefore, untargeted metabolomics, a technique facilitating the simultaneous exploration of multiple molecules in a biological sample employing $^1\text{H-NMR}$ and LC-HRMS/MS, was implemented. This approach enabled the relative quantification and identification of 133 metabolites (67 and 84 by $^1\text{H-NMR}$ and LC-HRMS/MS, respectively) in post-larvae exposed to noise. Notably, only 18 compounds were found to be common to both instrumental methods, which had similar individual classification performances (Figs. S3 & S4). A multiblock OPLS-DA with an explicative ability (R^2Y) of 1.00 and a predictive ability (Q^2) of 0.98 for a CV-ANOVA of 0.0010 was fitted to reveal the alterations induced to the larval metabolome by exposure to the ship noise at a high level ($n = 5$) (Fig. 5a,b; Table S4). This model, composed of 1 predictive and 1 orthogonal component, included 26 metabolites (11 detected by $^1\text{H-NMR}$, 13 by LC-HRMS/MS, and 2 by both methods). It was able to discriminate the larvae under control conditions and those exposed to all of

the noise levels, thus confirming that the metabolites included in the model are effectively correlated to the noise level. The discriminant metabolites included 15 amino acids, 4 nucleosides and derivatives, 2 cholines, and 5 other molecules, including 1 prostaglandin.

This untargeted exploration of the impact of noise on the metabolome of post-larvae was completed by a systematic characterization of the amino acid and energy metabolism, based on the absolute quantifica-

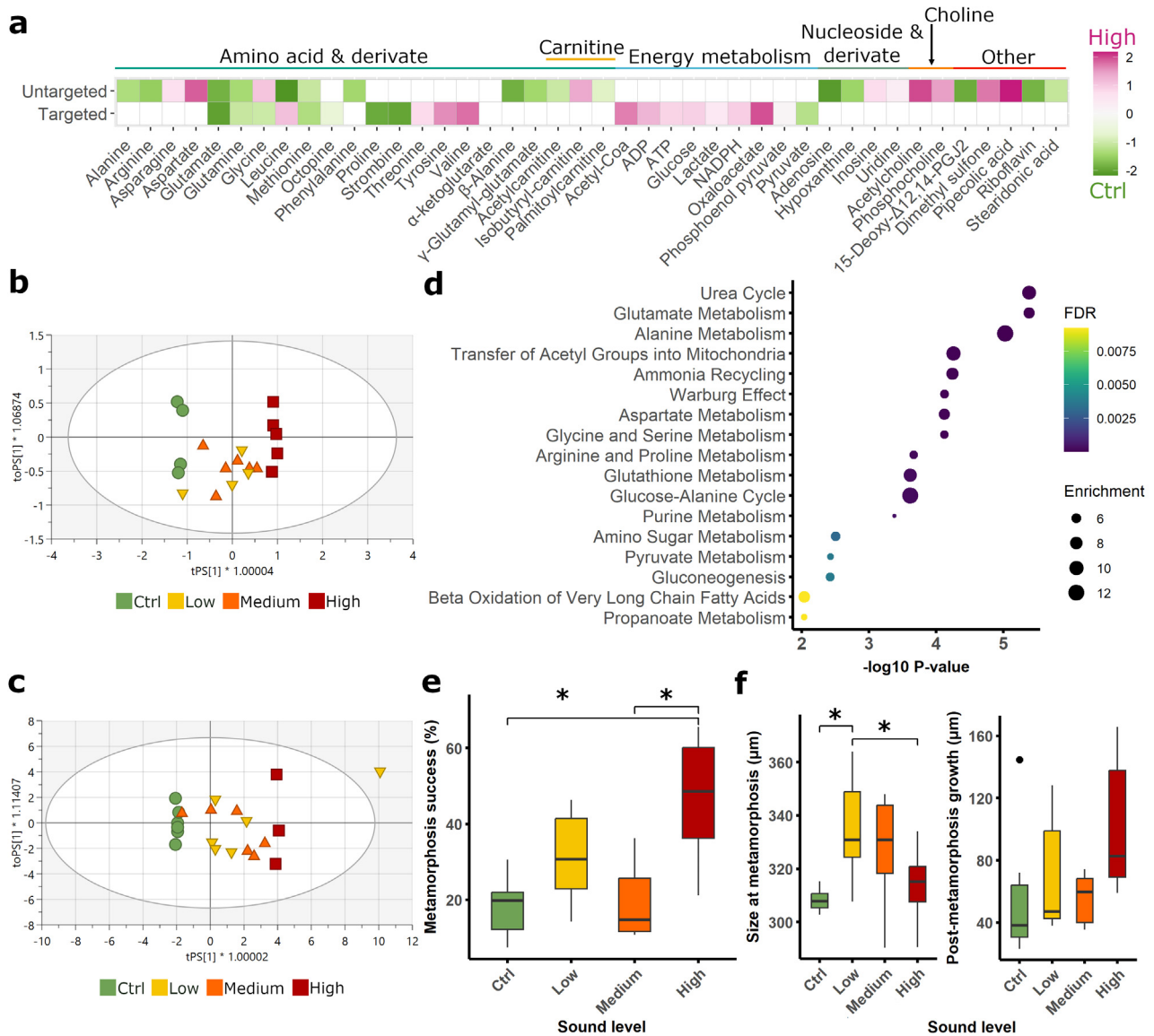


Fig. 5. Impact of shipping noise on amino acids, energy and oxidative metabolism in blue mussel post-larvae. Shipping noise treatment groups are control (Ctrl; ambient noise), low (~ 121 re $1 \mu\text{Pa}$), medium (~ 127 re $1 \mu\text{Pa}$), and high (~ 151 re $1 \mu\text{Pa}$). (a) Contribution of the metabolites identified by the multiblock OPLS-DA-based screening of the untargeted proton nuclear magnetic resonance ($^1\text{H-NMR}$) and mass spectrometry (MS) data, as well of the targeted LC-MS data. (b) Multi-block OPLS-DA scores plot based on the fitted model ($R^2\text{Y} = 1.00$, $Q^2 = 0.98$, $\text{CV-ANOVA} = 0.0010$) on untargeted $^1\text{H-NMR}$ and MS data. Ctrl $n = 4$, low $n = 4$, medium $n = 6$, high $n = 5$. (c) OPLS-DA scores plot based on the fitted model ($R^2\text{Y}_{\text{cum}} = 1.00$, $Q^2_{\text{cum}} = 0.99$, $\text{CV-ANOVA} = 0.0245$) on the targeted LC-MS amino acid and energy metabolism data. Ctrl $n = 6$, low $n = 6$, medium $n = 6$, high $n = 3$. (d) Metabolite set enrichment analysis performed using the list of metabolites obtained from the untargeted and targeted metabolomics OPLS-DA models. The bubble sizes represent the fold enrichment of the metabolic pathways identified, and the blue colour gradient corresponds to the p-value corrected for the false discovery rate (FDR). (e) Percentage of metamorphosis success of the larvae exposed to different noise levels ($*p < 0.05$). Each treatment $n = 6$. (f) Size of the larvae at the metamorphosis stage prodissoconch II (PII) and their post-metamorphosis growth ($*p < 0.05$, outliers are represented by dots). Each treatment $n = 6$. In e and f, boxplots show minimum and maximum values (whiskers), first and third quartiles (box), and median (horizontal line)

tion of a set of 48 metabolites (Table S5). These metabolites were subjected to a multivariate screening, as performed with the untargeted data set, to identify the molecules with concentrations affected by exposure to the high shipping noise level. Twenty metabolites were conserved in the OPLS-DA model com-

posed of 1 predictive and 3 orthogonal components ($R^2\text{Y}_{\text{cum}} = 1.00$, $Q^2_{\text{cum}} = 0.99$, $\text{CV-ANOVA} = 0.0245$) (Fig. 5c; Table S6). Five of these metabolites (all of which were amino acids) were also conserved in the untargeted model (glutamate, glutamine, glycine, leucine and methionine; Fig. 5a).

The impact on biochemical pathways of the mussel post-larvae following exposure to noise during metamorphosis was determined by metabolite set enrichment analysis (Fig. 5d) based on the combination of the discriminant metabolites identified in the untargeted and targeted approaches. This analysis highlighted 17 pathways significantly enriched in metabolites (FDR $p < 0.01$). Among them, pathways related to amino acids, including the urea cycle, glutamate and alanine metabolism, were the most extensively impacted. They were followed by pathways connected to energy metabolism, such as the transfer of acetyl groups into mitochondria, the Warburg effect (anaerobic glycolysis), pyruvate metabolism, gluconeogenesis, as well as β -oxidation of very long chain FAs. Finally, the oxidative stress response via glutathione metabolism was also affected.

3.3. Post-larval performance

Post-larval performances were evaluated using a Keyence VHX-2000 Series digital microscope. Those observations showed that the success of metamorphosis increased significantly with the sound treatment (+21% high vs. control, $p = 0.01$) in mussels sampled on collectors (Fig. 5e). Furthermore, the size at metamorphosis (PII measurements) (Fig. 5f) was significantly impacted by the noise (+18 μm low vs. control, $p = 0.02$, -17 μm low vs. high, $p = 0.04$) while the post-metamorphosis growth (D) did not differ significantly between the sound treatments (Fig. 5f).

4. DISCUSSION

4.1. Noise treatment

We used the noise profile of a single ship, the loudest vessel in the archipelago of St-Pierre-et-Miquelon, consistent with measurements of commercial ships (McKenna et al. 2012), aiming at standardizing the anthropogenic sound exposure to ensure that the primary variable in the experiment was the intensity of the noise. While a broader acoustic landscape might more accurately reflect real-world conditions, such an approach would require a long-duration sound file, which could be challenging given the brief lifespans of the larval stages studied. Furthermore, previous calibration work on the Larvosonic system revealed that both kinetic (particle velocity) and potential (pressure) energy decrease proportionally as source levels increase (Olivier et al. 2023).

Given this uniform decrease across treatments, the design ensured that trends in exposure levels (low, medium, high) were consistent between pressure and particle motion which is valuable, since mussels are likely to respond to particle motion rather than sound pressure (Popper & Hawkins 2018).

4.2. Shipping noise impact on post-larval metabolism

Noise modified the life cycle of mussel larvae by stimulating their settlement and modulating their metabolome. Those alterations may result from a direct effect of the sound or different level of metamorphosis development, including tissue morphology, induced by the sound treatment.

4.2.1. Modification of PUFA oxidation patterns indicated an inflammatory response

The responses to noise-induced stress triggered a modification of the production of lipid mediators (oxylipins and prostaglandins) by oxidation of PUFAs through direct interaction with reactive oxygen species (ROS), produced during oxidative stress, or ROS-activated enzymatic pathways, i.e. cyclooxygenase, lipoxygenase, and cytochrome P450. Therefore, noise could induce, directly or indirectly through the regulation of the metamorphosis process, a modification of lipid mediator patterns known to play essential roles in inflammation, reproduction, ion flux regulation, thermoregulation, and activation of the immune response in aquatic invertebrates (Canesi et al. 2002, Gagné et al. 2007, Di Costanzo et al. 2019). Several oxylipins and prostaglandins were retained in the OPLS-DA, which could suggest a modification of the pro-inflammatory/pro-resolving balance, although their role in stress and inflammation in aquatic organisms is not well understood (Gabbs et al. 2015).

Besides these physiological processes, oxylipin and CyPG levels may also affect larval development, especially during metamorphosis. Indeed, metamorphosis is associated with the development of juvenile-specific structures, including loss of the velum and development of the gills (Yang et al. 2013). During this transition, the innate immune system is solicited for the resorption and reorganization of larval tissues through the ROS-regulated process (Redza-Dutoridoir & Averill-Bates 2016) of apoptosis and ROS-generating phagocytosis which may impact the lipid oxidation patterns of the post-larvae (Winston et al.

1996, Davidson & Swalla 2002, Wang et al. 2023). Interestingly, CyPGs and oxylipins may also be involved in the settlement of marine invertebrates (Knight et al. 1999), suggesting that elevated ship noise levels could trigger this action on larvae, with potential impacts on ecosystems as well as on aquaculture.

Overall, noise-induced stress appeared to modulate the production of lipid mediators from PUFAs, possibly leading to different inflammatory profiles between control and noise-exposed post-larvae. However, it was not clear whether its impact was direct or linked to different ontogenetic development at metamorphosis.

4.2.2. Energy requirements and protein turnover impacts on nervous system activity

Gluconeogenesis and energy production is increased in post-larvae exposed to noise. Amino acids and their derivatives, comprising 22 out of 42 compounds affected by noise in both untargeted and targeted metabolomes, showed significant changes, akin to the response observed in adult mussels when exposed to pollutants, leading to stress and reduced feeding rates (Wale et al. 2019) due to a reduction in valve gape opening (Day et al. 2017, Ledoux et al. 2023). In response to food restriction, mussels increased gluconeogenesis to produce glucose from oxidizable amino acids, which helps maintain intracellular osmolarity (Moyes et al. 1990). Consequently, lower levels of alanine, arginine, glutamate, glutamine, methionine, phenylalanine, and proline in noise-exposed post-larvae suggest higher oxidation rates to compensate for reduced feeding (Spiga et al. 2016) and greater energy demands caused by noise-related stress and the extension of the prospecting pelagic phase (Vazzana et al. 2016, Gigot et al. 2023).

Additionally, lipid β -oxidation may be heightened in noise-exposed post-larvae, indicated by lower levels of certain acylcarnitines, such as acetylcarnitine and palmitoylcarnitine, suggesting increased transport of FAs into mitochondria for breakdown, generating glucose and energy (Longo et al. 2016). This elevated gluconeogenesis rate led to higher glucose levels and greater depletion of glycolysis products (pyruvate, phosphoenolpyruvate), accompanied by increased levels of ATP, ADP, and Krebs cycle intermediates (acetyl-CoA, oxaloacetate, α -ketoglutarate), reflecting intensified aerobic energy production and amino acid turnover. The aerobic energy production is complemented by the transformation via the anaerobic glycolysis of glucose into lactate, which was higher in post-larvae exposed to noise.

However, the levels of octopine (a derivative of arginine and alanine) and strombine [N-(carboxymethyl)-D-alanine] involved in maintaining the redox balance under anaerobic conditions and anaerobic respiration end-products, respectively, were higher in the controls, suggesting higher energy demands. These findings indicate lower metamorphosis development in the control group, as evidenced by morphometric data, correlating with metabolic activity, specifically the NADH/NAD⁺ ratio. The elevated ratio observed in the high sound condition may suggest an increased reliance on anaerobic metabolism, potentially related to the demands of gill development and/or the stress induced by sound exposure.

Protein and cellular turnover increased in post-larvae exposed to noise. In post-larvae exposed to noise, 5 proteogenic amino acids (asparagine, aspartate, threonine, tyrosine, valine) were found at higher levels. Threonine, tyrosine, aspartate, and asparagine may be precursors for the biosynthesis of new proteins in response to the stress-induced formation of ROS provoking protein damage or the increased protein demand for the remodelling occurring during metamorphosis. The branched-chain amino acid valine is essential for the immune system by providing energy and being a precursor for the biosynthesis of protective molecules (Calder 2006), but it also plays an important role in the regulation of protein turnover processes, as observed in *Mytilus galloprovincialis* challenged by *Vibrio anguillarum* (Ji et al. 2013). The post-larval immune system is likely to be triggered by the response to stress, involving prostaglandins and oxylipins (Canesi et al. 2002). The exposure of mussel larvae to noise, or the regulation of their metamorphosis by noise, may thus have an impact on their protein turnover, in combination with a higher energy level due to increased gluconeogenesis, which could lead to a tendency to grow faster after metamorphosis (Fig. 5f).

Action on nervous system activity. The level of the neurotransmitter acetylcholine — which plays an important role in the cholinergic system involved in digestion, control of the heartbeat, and movement — is dependent on its rate of inactivation via hydrolysis into choline by acetylcholinesterase (AChE). The activity of this enzyme is considered the most effective biomarker in assessing neurological changes caused by xenobiotics (Fontes et al. 2022). The higher level of acetylcholine (decreased hydrolysis by AChE) in post-larvae exposed to noise, which is consistent with the decrease of AChE activity after exposure to pollutants such as cocaine (Fontes et al. 2022) and the typical decreased enzyme activity in mussels exposed to environmental stress (Ricciardi et al. 2006), could have a stimulatory

effect. The formation of ROS might be the cause of the decreased hydrolysis by AchE similarly to what has been observed during the exposure of mussels to waste water (Gagné et al. 2011). Acetylcholine is also an inhibitor of some ctenidial lateral cilia that reduce water pumping rate in *Mytilus edulis* (Jones & Richards 1993), in good agreement with the reduced respiration and feeding rates observed during noise exposure (Wale et al. 2019). Additionally, this neurotransmitter induces both settlement behaviour and metamorphosis development in bivalves (Beiras & Widdows 1995, Bayne 2017). Its higher level in post-larvae exposed to noise could therefore explain the increased settlement level and faster metamorphosis development.

4.3. Noise induces settlement in bad habitats and in an altered physiological condition

Competent veliger mussel larvae can delay their metamorphosis and remain adrift up to a size of 400 μm , an almost 100% increase from the 230 μm observed for the most precocious individuals, due to potential absence of a suitable environment required for stimulating settlement, thus forcing larvae to continue planktonic growth (Martel et al. 2014). At an average size of 300 μm , the larvae were already in a delayed metamorphosis condition, undoubtedly linked to the absence of turbulence in the Larvasonic systems to limit noise perturbation (Olivier et al. 2023). Indeed, settlement success is positively correlated with centrifugal and advective flow velocity and turbulence (Pernet et al. 2003). As highlighted by the metabolomic characterization, post-larvae exposed to high sound levels had higher energy expenditures than the others, which potentially results in a decrease in energy reserves and therefore activates the oxidative energy pathways. Those larvae would thus consume considerably more energy daily than the others (Bayne 1965, Gigot et al. 2023), which would result in them becoming 'desperate larvae' faster (Knight-Jones 1951, Toonen & Pawlik 1994), i.e. forced to settle without any positive settlement cue, or even in an unfavourable environment, at a smaller size. Alternatively, a second hypothesis could be that there existed a disparity in the metamorphosis stage of the larvae between the control and high sound exposure groups and that the latter may have exhibited a more advanced metamorphic state compared to the former (Cannuel et al. 2009).

In summary, marine traffic noise delays metamorphosis, leading to post-larval size differences, while increasing its success in a suboptimal habitat. The post-

larvae that settled and underwent metamorphosis in this suboptimal habitat showed increased metabolomic demands and an altered prostaglandin profile, indicating stress and inflammatory responses, which may reduce their chances of survival. However, these results need to be enriched by long-term studies.

4.4. Perspectives for sessile bivalve aquaculture, ecosystems, and regulations

Anthropogenic noise, associated with maritime traffic, modulates larval metamorphosis dynamics and recruitment processes, potentially altering larval selectivity and decreasing survival rates to adulthood, with potential cascading effects on population dynamics and marine biodiversity (Pechenik 2006, Gigot et al. 2023). Those perturbations may additionally carry socio-economic implications, particularly for aquaculture systems reliant on spat capture (Kamerans & Capelle 2019). Our innovative approach coupling metabolomic monitoring of *Mytilus edulis* larvae stress responses and acoustic studies provides the first metabolic dose-response data about the impact of shipping noise on sessile bivalve development. These results could be used by regulators and decision-makers. Indeed, no binding regulations currently require the reduction of manmade underwater noise. There are some regulations and recommendations to help maritime professionals reduce noise pollution, but with limited legal status, such as the IMO Guidelines (Maruf & Chang 2023). Those initiatives are based on thresholds, defined by the noise level at which individual animals start to experience adverse effects, as is the case for the 'Level of Onset of Biological Adverse Effect (LOBE)' proposed by the European Union (Borsani et al. 2023). The definition of thresholds for a variety of organisms is crucial for the implementation of precautionary management and mitigation measures, such as the reduction of vessel speed (Lajaunie et al. 2023), the modulation of ship traffic and speed in reproduction zones during the spawning season, or the promotion of ship designs that reduce propeller, machinery, and flow noises (Arveson & Vendittis 2000), to limit the impacts on biodiversity and the management of fisheries and aquaculture.

4.5. Conclusion

This study highlights that marine traffic noise disrupts the metamorphosis and settlement of *Mytilus*

edulis larvae, resulting in size differences and increased stress-related metabolomic expenditures in suboptimal habitats. These findings emphasize the significant impact of anthropogenic noise on larval development, with potential negative effects on bivalve aquaculture, ecosystem health, and marine biodiversity.

Data availability. The untargeted metabolomic data sets generated and analysed during the current study are available in the MetaboLights repository hosted by the EMBL-EBI (Haug et al. 2020) at www.ebi.ac.uk/metabolights/MTBLS5678. All quantitative data extracted from the targeted metabolomics are provided as supplementary data. The soundtrack used during the experiment was deposited under the DOI 10.5281/zenodo.10910123 in the Zenodo repository (<https://zenodo.org>) hosted by the European Organization for Nuclear Research (CERN).

Acknowledgements. We acknowledge access, for method development purposes, to the biomolecular NMR platform of the Institut de biologie physico-chimique (IBPC) supported by the CNRS, the Labex DYNAMO (ANR-11-LABX-0011), the Equipex CACSICE (ANR-11-EQPX-0008), and the Conseil Régional d'Île-de-France (SESAME grant). We thank Delphine Mathias for her contribution to the recording of the shipping noise soundtrack; and Leanne Ohlund (UQAM), Nathalie Gauthier (UQAR-ISMER), and Mathieu Millour (Iso-BioKem Inc) for their technical support. D.V., S.B., B.G., F.O., D.E.W., I.M., and R.T. are members of the Ressources Aquatiques Québec Research Network. This study was funded by the Fonds de la Recherche du Québec Nature et Technologies (FRQNT 280057) and the Agence Nationale de la Recherche (ANR-19-FQSM-0005) through the French-Québec maritime funding program. Supplementary funds were also obtained from the Ressources Aquatiques Québec Research Network (FRQNT, #2014-RS-171172). This study is a contribution to the BeBEST2 International Research Project (CNRS INEE/LEMAR and UQAR-ISMER).

LITERATURE CITED

- Andrew RK, Howe BM, Mercer JA, Dzieciuch MA (2002) Ocean ambient sound: comparing the 1960s with the 1990s for a receiver off the California coast. *Acoust Res Lett Online* 3:65–70
- Arveson PT, Vendittis DJ (2000) Radiated noise characteristics of a modern cargo ship. *J Acoust Soc Am* 107: 118–129
- Bayne BL (1965) Growth and the delay of metamorphosis of the larvae of *Mytilus edulis* (L.). *Ophelia* 2:1–47
- Bayne BL (2017) *Biology of oysters*. Academic Press, London
- Beiras R, Widdows J (1995) Induction of metamorphosis in larvae of the oyster *Crassostrea gigas* using neuroactive compounds. *Mar Biol* 123:327–334
- Borsani J, Andersson M, Andre M, Azzellino A and others (2023) Setting EU threshold values for continuous underwater sound. Publications Office of the European Union, Luxembourg
- Borthagaray AI, Carranza A (2007) Mussels as ecosystem engineers: their contribution to species richness in a rocky littoral community. *Acta Oecol* 31:243–250
- Calder PC (2006) Branched-chain amino acids and immunity. *J Nutr* 136:288S–293S
- Canesi L, Scarpato A, Betti M, Ciacci C, Pruzzo C, Gallo G (2002) Bacterial killing by *Mytilus* hemocyte monolayers as a model for investigating the signaling pathways involved in mussel immune defence. *Mar Environ Res* 54: 547–551
- Cannuel R, Beninger PG, McCombie H, Boudry P (2009) Gill development and its functional and evolutionary implications in the blue mussel *Mytilus edulis* (Bivalvia: Mytilidae). *Biol Bull (Woods Hole)* 217:173–188
- Cervello G, Olivier F, Chauvaud L, Winkler G, Mathias D, Juanes F, Tremblay R (2023) Impact of anthropogenic sounds (pile driving, drilling and vessels) on the development of model species involved in marine biofouling. *Front Mar Sci* 10:111505
- Chauvaud S, Chauvaud L, Jolivet A (2018) Impacts des sons anthropiques sur la faune marine. Éditions Quae, Paris
- Conference of the Parties of the Convention on Migratory Species (2017) UNEP/CMS/Resolution 12.14, Adverse impacts of anthropogenic noise on cetaceans and other migratory species. <https://www.cms.int/en/document/adverse-impacts-anthropogenic-noise-cetaceans-and-other-migratory-species-0>
- Davidson B, Swalla BJ (2002) A molecular analysis of ascidian metamorphosis reveals activation of an innate immune response. *Development* 129:4739–4751
- Day RD, McCauley RD, Fitzgibbon QP, Hartmann K, Semmens JM (2017) Exposure to seismic air gun signals causes physiological harm and alters behavior in the scallop *Pecten fumatus*. *Proc Natl Acad Sci USA* 114: E8537–E8546
- de Soto NA, Delorme N, Atkins J, Howard S, Williams J, Johnson M (2013) Anthropogenic noise causes body malformations and delays development in marine larvae. *Sci Rep* 3:2831
- Di Costanzo F, Di Dato V, Ianora A, Romano G (2019) Prostaglandins in marine organisms: a review. *Mar Drugs* 17: 428
- Duarte CM, Chapuis L, Collin SP, Costa DP and others (2021) The soundscape of the Anthropocene ocean. *Science* 371: eaba4658
- Eriksson L, Trygg J, Wold S (2008) CV-ANOVA for significance testing of PLS and OPLS models. *J Chemometr* 22: 594–600
- European Union (2008) Directive 2008/56/EC of the European Parliament and of the Council of 17 June 2008 establishing a framework for community action in the field of marine environmental policy. *Off J Eur Union* 164:19–40
- FAO (2019) Aquaculture production by species and country or area: mussels. https://www.fao.org/fishery/static/Yearbook/YB2019_USBCard/root/aquaculture/b54.pdf (accessed on 17 May 2024)
- Fontes MK, Dourado PLR, de Campos BG, Maranhão LA, de Almeida EA, Abessa DM de S, Pereira CDS (2022) Environmentally realistic concentrations of cocaine in seawater disturbed neuroendocrine parameters and energy status in the marine mussel *Perna perna*. *Comp Biochem Physiol Part C Toxicol Pharmacol* 251:109198
- Frisk GV (2012) Noiseconomics: the relationship between ambient noise levels in the sea and global economic trends. *Sci Rep* 2:437

- ✦ Gabbs M, Leng S, Devassy JG, Monirujjaman M, Aukema HM (2015) Advances in our understanding of oxylipins derived from dietary PUFAs. *Adv Nutr* 6:513–540
- ✦ Gagné F, Gagnon C, Turcotte P, Blaise C (2007) Changes in metallothionein levels in freshwater mussels exposed to urban wastewaters: effects from exposure to heavy metals? *Biomark Insights* 2:107–116
- ✦ Gagné F, André C, Cejka P, Hausler R, Fournier M (2011) Evidence of neuroendocrine disruption in freshwater mussels exposed to municipal wastewaters. *Sci Total Environ* 409:3711–3718
- ✦ Gigot M, Olivier F, Cervello G, Tremblay R and others (2023) Pile driving and drilling underwater sounds impact the metamorphosis dynamics of *Pecten maximus* (L., 1758) larvae. *Mar Pollut Bull* 191:114969
- ✦ Hadfield MG (2000) Why and how marine-invertebrate larvae metamorphose so fast. *Semin Cell Dev Biol* 11:437–443
- Hadfield MG, Paul VJ (2001) Natural chemical cues for settlement and metamorphosis of marine-invertebrate larvae. In: McClintock JB, Baker BJ (eds) *Marine chemical ecology*. CRC Press, Boca Raton, FL, p 431–461
- ✦ Haug K, Cochrane K, Nainala VC, Williams M, Chang J, Jayaseelan KV, O'Donovan C (2020) MetaboLights: a resource evolving in response to the needs of its scientific community. *Nucleic Acids Res* 48:D440–D444
- ✦ Hawkins AD, Popper AN (2017) A sound approach to assessing the impact of underwater noise on marine fishes and invertebrates. *ICES J Mar Sci* 74:635–651
- ✦ IMO (International Maritime Organization) (2023) Revised guidelines for the reduction of underwater radiated noise from shipping to address adverse impacts on marine life, MEPC.1/Circ.906, 22 August 2023. IMO, London
- ✦ Jacob D, Deborde C, Lefebvre M, Maucourt M, Moing A (2017) NMRProcFlow: a graphical and interactive tool dedicated to 1D spectra processing for NMR-based metabolomics. *Metabolomics* 13:36
- ✦ Jalkanen JP, Johansson L, Andersson MH, Majamäki E, Sigra P (2022) Underwater noise emissions from ships during 2014–2020. *Environ Pollut* 311:119766
- ✦ Ji C, Wu H, Wei L, Zhao J, Wang Q, Lu H (2013) Responses of *Mytilus galloprovincialis* to bacterial challenges by metabolomics and proteomics. *Fish Shellfish Immunol* 35:489–498
- ✦ Jolivet A, Tremblay R, Olivier F, Gervaise C, Sonier R, Genard B, Chauvaud L (2016) Validation of trophic and anthropic underwater noise as settlement trigger in blue mussels. *Sci Rep* 6:33829
- ✦ Jones HD, Richards OG (1993) The effects of acetylcholine, dopamine and 5-hydroxytryptamine on water pumping rate and pressure in the mussel *Mytilus edulis* L. *J Exp Mar Biol Ecol* 170:227–240
- ✦ Joyce A, Vogeler S (2018) Molluscan bivalve settlement and metamorphosis: neuroendocrine inducers and morphogenetic responses. *Aquaculture* 487:64–82
- Kamermans P, Capelle JJ (2019) Provisioning of mussel seed and its efficient use in culture. In: Smaal AC, Ferreira JG, Grant J, Petersen JK, Strand Ø (eds) *Goods and services of marine bivalves*. Springer International Publishing, Cham, p 27–49
- ✦ Kim W, Jang JH, Zhong X, Seo H, Surh YJ (2021) 15-Deoxy-12,14-Prostaglandin J2 promotes resolution of experimentally induced colitis. *Front Immunol* 12:615803
- ✦ Knight J, Rowley AF, Yamazaki M, Clare AS (1999) Eicosanoids are modulators of larval settlement in the barnacle, *Balanus amphitrite*. *J Mar Biol Assoc UK* 80:113–117
- ✦ Knight-Jones EW (1951) Gregariousness and some other aspects of the settling behaviour of *Sipiroboris*. *J Mar Biol Assoc UK* 30:201–222
- ✦ Lajaunie M, Ollivier B, Ceyrac L, Dellong D, Le Courtois F (2023) Large-scale simulation of a shipping speed limitation measure in the Western Mediterranean Sea: effects on underwater noise. *J Mar Sci Eng* 11:251
- ✦ Ledoux T, Clements JC, Comeau LA, Cervello G and others (2023) Effects of anthropogenic sounds on the behavior and physiology of the Eastern oyster (*Crassostrea virginica*). *Front Mar Sci* 10:1104526
- ✦ Lee SY, Ahn JH, Ko KW, Kim J and others (2010) Prostaglandin A2 activates intrinsic apoptotic pathway by direct interaction with mitochondria in HL-60 cells. *Prostaglandins Other Lipid Mediat* 91:30–37
- ✦ Lee BR, Paing MH, Sharma-Walia N (2021) Cyclopentenone prostaglandins: biologically active lipid mediators targeting inflammation. *Front Physiol* 12:640374
- ✦ Lillis A, Eggleston DB, Bohnenstiehl DR (2013) Oyster larvae settle in response to habitat-associated underwater sounds. *PLOS ONE* 8:e79337
- ✦ Longo N, Frigeni M, Pasquali M (2016) Carnitine transport and fatty acid oxidation. *Biochim Biophys Acta* 1863:2422–2435
- ✦ Martel AL, Hynes TM, Buckland-Nicks J (1995) Prodissoconch morphology, planktonic shell growth, and size at metamorphosis in *Dreissena polymorpha*. *Can J Zool* 73:1835–1844
- ✦ Martel AL, Tremblay R, Toupoint N, Olivier F, Myrand B (2014) Veliger size at metamorphosis and temporal variability in prodissoconch II morphometry in the blue mussel (*Mytilus edulis*): potential impact on recruitment. *J Shellfish Res* 33:443–455
- ✦ Maruf, Chang YC (2023) Further development of the Law of the Sea Convention in the Anthropocene era: the case of anthropogenic underwater noise. *Sustainability* 15:9461
- ✦ McDonald MA, Hildebrand JA, Wiggins SM (2006) Increases in deep ocean ambient noise in the Northeast Pacific west of San Nicolas Island, California. *J Acoust Soc Am* 120:711–718
- ✦ McKenna MF, Ross D, Wiggins SM, Hildebrand JA (2012) Underwater radiated noise from modern commercial ships. *J Acoust Soc Am* 131:92–103
- ✦ Moyes CD, Suarez RK, Hochachka PW, Ballantyne JS (1990) A comparison of fuel preferences of mitochondria from vertebrates and invertebrates. *Can J Zool* 68:1337–1349
- ✦ Olivier F, Gigot M, Mathias D, Jezequel Y and others (2023) Assessing the impacts of anthropogenic sounds on early stages of benthic invertebrates: the 'Larvosonic system.'. *Limnol Oceanogr Methods* 21:53–68
- ✦ Pang Z, Chong J, Zhou G, De Lima Morais DA and others (2021) MetaboAnalyst 5.0: narrowing the gap between raw spectra and functional insights. *Nucleic Acids Res* 49:W388–W396
- ✦ Pechenik JA (1990) Delayed metamorphosis by larvae of benthic marine invertebrates: Does it occur? Is there a price to pay? *Ophelia* 32:63–94
- ✦ Pechenik JA (2006) Larval experience and latent effects—metamorphosis is not a new beginning. *Integr Comp Biol* 46:323–333
- Pelo R, Wootton D (2004) Maritime traffic distribution in Atlantic Canada to support an evaluation of a Sensitive Sea Area proposal. MARIN Report #2004-06, Dalhousie University, Department of Industrial Engineering, Halifax, NS

- Peng C, Zhao X, Liu S, Shi W and others (2016) Effects of anthropogenic sound on digging behavior, metabolism, $\text{Ca}^{2+}/\text{Mg}^{2+}$ ATPase activity, and metabolism-related gene expression of the bivalve *Sinonovacula constricta*. *Sci Rep* 6:24266
- Pernet F, Tremblay R, Bourget E (2003) Settlement success, spatial pattern and behavior of mussel larvae *Mytilus* spp. in experimental 'downwelling' systems of varying velocity and turbulence. *Mar Ecol Prog Ser* 260:125–140
- Popper AN, Hawkins AD (2018) The importance of particle motion to fishes and invertebrates. *J Acoust Soc Am* 143: 470–488
- Rayssac N, Pernet F, Lacasse O, Tremblay R (2010) Temperature effect on survival, growth, and triacylglycerol content during the early ontogeny of *Mytilus edulis* and *M. trossulus*. *Mar Ecol Prog Ser* 417:183–191
- Redza-Dutordoir M, Averill-Bates DA (2016) Activation of apoptosis signalling pathways by reactive oxygen species. *Biochim Biophys Acta Mol Cell Res* 1863: 2977–2992
- Ricciardi F, Binelli A, Provini A (2006) Use of two biomarkers (CYP450 and acetylcholinesterase) in zebra mussel for the biomonitoring of Lake Maggiore (northern Italy). *Ecotoxicol Environ Saf* 63:406–412
- Roberts L, Cheesman S, Breithaupt T, Elliott M (2015) Sensitivity of the mussel *Mytilus edulis* to substrate-borne vibration in relation to anthropogenically generated noise. *Mar Ecol Prog Ser* 538:185–195
- Schmidlin S, Parcerisas C, Hubert J, Watson MS and others (2024) Comparison of the effects of reef and anthropogenic soundscapes on oyster larvae settlement. *Sci Rep* 14:12580
- Smaal AC, Ferreira JG, Grant J, Petersen JK, Strand Ø (eds) (2019) Goods and services of marine bivalves. Springer International Publishing, Cham
- Solé M, Kaifu K, Mooney TA, Nedelec SL and others (2023) Marine invertebrates and noise. *Front Mar Sci* 10: 1129057
- Spiga I, Caldwell GS, Brintjes R (2016) Influence of pile driving on the clearance rate of the blue mussel, *Mytilus edulis* (L.). *Proc Meet Acoust* 27:040005
- Statistics Canada (2019) Production d'aquaculture en quantité et en valeurs. <https://www.dfo-mpo.gc.ca/stats/aqua/aqua19-fra.htm>
- Toonen RJ, Pawlik JR (1994) Foundations of gregariousness. *Nature* 370:511–512
- United Nations (1982) United Nations Convention on the Law of the Sea. Part XII Protection and preservation of the marine environment. https://www.un.org/Depts/los/convention_agreements/convention_overview_convention.htm
- Vazzana M, Celi M, Maricchiolo G, Genovese L and others (2016) Are mussels able to distinguish underwater sounds? Assessment of the reactions of *Mytilus galloprovincialis* after exposure to lab-generated acoustic signals. *Comp Biochem Physiol A Mol Integr Physiol* 201:61–70
- Wale MA, Briers RA, Hartl MGJ, Bryson D, Diele K (2019) From DNA to ecological performance: effects of anthropogenic noise on a reef-building mussel. *Sci Total Environ* 689:126–132
- Wang YQ, Liu Q, Zhou Y, Chen L and others (2023) Stage-specific transcriptomes of the mussel *Mytilus coruscus* reveals the developmental program for the planktonic to benthic transition. *Genes* 14:287
- Wilkens SL, Stanley JA, Jeffs AG (2012) Induction of settlement in mussel (*Perna canaliculus*) larvae by vessel noise. *Biofouling* 28:65–72
- Winston GW, Moore MN, Kirchin MA, Soverchia C (1996) Production of reactive oxygen species by hemocytes from the marine mussel, *Mytilus edulis*: lysosomal localization and effect of xenobiotics. *Comp Biochem Physiol C Pharmacol Toxicol Endocrinol* 113:221–229
- Worley B, Powers R (2016) PCA as a practical indicator of OPLS-DA model reliability. *Curr Metabolomics* 4: 97–103
- Xia J, Wishart DS (2010) MSEA: a web-based tool to identify biologically meaningful patterns in quantitative metabolomic data. *Nucleic Acids Res* 38:W71–W77
- Yang JL, Shen PJ, Liang X, Li YF, Bao WY, Li JL (2013) Larval settlement and metamorphosis of the mussel *Mytilus coruscus* in response to monospecific bacterial biofilms. *Biofouling* 29:247–259

Editorial responsibility: Craig Radford,
Warkworth, New Zealand
Reviewed by: L. Auken and 2 anonymous referees

Submitted: August 15, 2024
Accepted: February 13, 2025
Proofs received from author(s): April 9, 2025

Table S1. Table of equivalent sound levels in sound pressure level (total root-mean-square Sound Pressure Level SPL_{RMS}) measured.

Sound pressure level (SPL) RMS measured (dB re 1 μPa)				
Conditions	Arrival	Departure	Mean	SE
Control	117.0	115.8	116.4	0.8
Low	124.3	118.2	121.3	4.3
Medium	128.8	125.3	127.1	2.5
High	152.6	149.2	150.9	2.4

$$TL = 15 \log_{10}(x)$$

$$170 - 151 = 15 \log_{10}(x)$$

$$19 = 15 \log_{10}(x)$$

$$\frac{19}{15} = 10^x$$

$$x = 10^{\frac{19}{15}}$$

$$x = 18.47 \text{ m}$$

Fig. S1. Calculation of the estimation of the transmission loss (TL) of the different sound intensities to evaluate the exposure distance (x) from the source (cargo-ship). Example of calculation for high sound exposure at 151 dB. Based on the original in situ sound recordings, we hypothesised a vessel noise source level of 170 dB re 1 μPa.

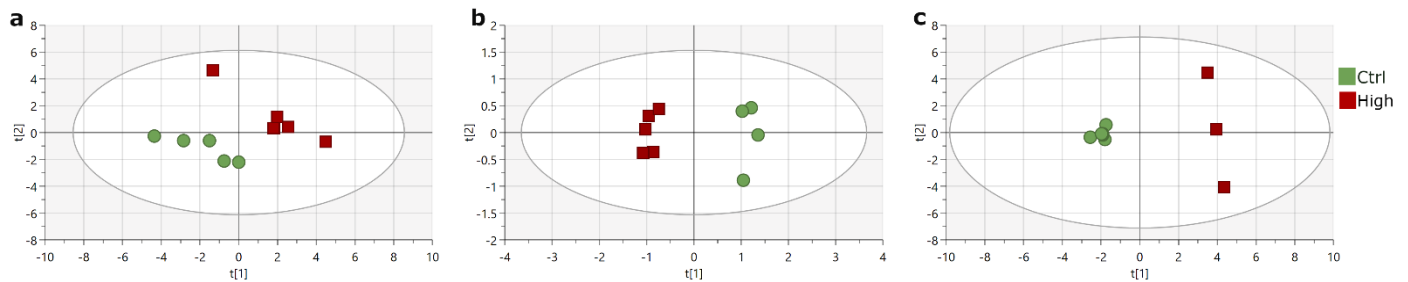


Fig. S2. Principal component analysis (PCA) adjusted to the set of metabolites, from blue mussel post-larvae, selected by multivariate OPLS-DA screening showing that supervised OPLS-DA as well as non-supervised PCA methods are able to cluster the pools of larvae in function of the intensity of the noise. Therefore, the set of metabolites included in the models are able to explain the variations related to the sound treatments. Green circles: control, red boxes: high shipping noise. **a**, PCA fitted to the set of metabolites included in the OPLS-DA adjusted to the targeted prostaglandin, oxidant metabolism data. The PCA is composed of four components with the two first one explaining 79% of the variability in the metabolite set. **b**, PCA fitted to the set of metabolites included in the OPLS-DA adjusted to the untargeted approach data. The PCA is composed of two components with the first one explaining 62% of the variability in the metabolite set. **c**, PCA fitted to the set of metabolites included in the OPLS-DA adjusted to the targeted amino-acids, energy metabolism data. The PCA is composed of two components explaining 65% of the variability in the metabolite set.

Table S2. Targeted LC-MS-based quantification (mean \pm standard error ng/g) of prostaglandin and unsaturated fatty oxidation products in blue mussel post-larvae. The significance of the differences in concentrations of the metabolites between noise levels was tested by Permanova (P-value < 0.05). Significant differences of concentration are indicated by letters.

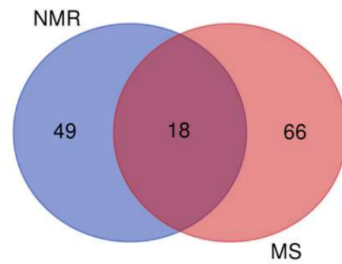
Metabolite	Control	Low	Medium	High
Cyclopentenone prostaglandin				
PGE2	375 \pm 116	246 \pm 31	280 \pm 27	225 \pm 36
PGD2	212 \pm 57	188 \pm 15	155 \pm 24	234 \pm 63
PGA2	27 \pm 4^b	22 \pm 2^b	52 \pm 5^a	36 \pm 6^{ab}
PGJ2	194 \pm 24	169 \pm 24	169 \pm 8	150 \pm 19
15-deoxy-d12,14-PGJ2	237 \pm 29	260 \pm 68	281 \pm 50	156 \pm 14
11b_PGF2a	37 \pm 5	28 \pm 3	39 \pm 7	24 \pm 4
15-keto-PGE2	20 \pm 3	20 \pm 3	17 \pm 4	12 \pm 2
15-keto-PGF2 α	286 \pm 36^a	244 \pm 27^a	228 \pm 33^a	88 \pm 14^b
13,14-dihydro-15-Keto-PGE2	86 \pm 11	75 \pm 12	65 \pm 7	80 \pm 14
13,14-dihydro-15-Keto-PGD2	465 \pm 133	350 \pm 47	287 \pm 25	335 \pm 42
13,14-dihydro-15-Keto-PGF2 α	79 \pm 9	78 \pm 14	113 \pm 18	83 \pm 18
EPA oxylipin				
PGE3	49 \pm 4	56 \pm 10	45 \pm 12	30 \pm 8
PGF3 α	66 \pm 19	65 \pm 8	61 \pm 11	61 \pm 10
5-HEPE	315 \pm 19	325 \pm 30	384 \pm 55	290 \pm 29
8-HEPE	2111 \pm 100	1746 \pm 166	1883 \pm 181	1571 \pm 130
9-HEPE	353 \pm 104^a	155 \pm 26^{ab}	150 \pm 27^{ab}	100 \pm 14^b
11-HEPE	1275 \pm 82^a	830 \pm 133^b	719 \pm 51^b	575 \pm 100^b
18-HEPE	3182 \pm 492	3670 \pm 348	4604 \pm 428	3032 \pm 416
12-HEPE	362 \pm 96	223 \pm 25	213 \pm 9	227 \pm 28
15-HEPE	661 \pm 76	557 \pm 36	529 \pm 50	466 \pm 50
ALA-GLA-oxylipin				
9(S)-HOTrE	270 \pm 41^b	301 \pm 47^b	499 \pm 43^a	302 \pm 44^b
13(S)-HOTrE	91 \pm 10	83 \pm 15	67 \pm 11	64 \pm 16
13(S)-HOTrE(g)	54 \pm 8	52 \pm 8	63 \pm 6	49 \pm 11
Arachidonic-oxylipin				
11-HETE	425 \pm 24	338 \pm 54	403 \pm 29	314 \pm 44
12-HETE	211 \pm 29	165 \pm 26	175 \pm 10	160 \pm 21
15-HETE	77 \pm 21	85 \pm 12	66 \pm 15	49 \pm 12
8-HETE	562 \pm 37	464 \pm 63	536 \pm 61	459 \pm 40
9-HETE	106 \pm 15	98 \pm 13	97 \pm 10	75 \pm 10
5-HETE	68 \pm 3	62 \pm 4	69 \pm 6	61 \pm 7
15-oxoHETE	349 \pm 110	224 \pm 25	209 \pm 9	225 \pm 29
Linoleic-oxylipin				
(\pm)12(13)-DiOME	14 \pm 1	11 \pm 2	14 \pm 3	11 \pm 4
(\pm)9(10)-DiHOME	11 \pm 1	9 \pm 2	10 \pm 2	7 \pm 1
13-oxoODE	108 \pm 9	103 \pm 11	110 \pm 13	96 \pm 12
9-oxoODE	191 \pm 10	174 \pm 27	166 \pm 29	165 \pm 23
13-HODE	155 \pm 18	152 \pm 18	183 \pm 15	147 \pm 27
9-HODE	435 \pm 169	123 \pm 25	186 \pm 84	103 \pm 21
(\pm)12(13)-EpOME	61 \pm 21	23 \pm 5	24 \pm 5	49 \pm 25
(\pm)9(10)-EpOME	458 \pm 64	358 \pm 52	449 \pm 114	352 \pm 75
HDHA-oxylipin				
22-HDHA	16 \pm 4	17 \pm 3	17 \pm 4	20 \pm 5
20-HDHA	305 \pm 73	381 \pm 31	507 \pm 22	401 \pm 97
17-HDHA	1071 \pm 126	908 \pm 93	896 \pm 69	731 \pm 96
16-HDHA	177 \pm 29	194 \pm 45	242 \pm 17	269 \pm 66
13-HDHA	648 \pm 36^a	307 \pm 74^b	224 \pm 29^b	212 \pm 45^b
14-HDHA	359 \pm 71	298 \pm 39	309 \pm 21	313 \pm 43
10-HDHA	282 \pm 33	290 \pm 44	321 \pm 34	270 \pm 31
11-HDHA	217 \pm 103	111 \pm 23	111 \pm 25	69 \pm 9
7-HDHA	73 \pm 3	73 \pm 9	72 \pm 5	58 \pm 5
8-HDHA	759 \pm 25	582 \pm 136	601 \pm 70	403 \pm 58
4-HDHA	57 \pm 4	47 \pm 6	49 \pm 6	39 \pm 8

Table S3. Contribution and importance of the variables in the projection (VIP) of the metabolites included in the OPLS-DA model ($R^2Y=0.97$, $Q^2=0.95$, $CV\text{-ANOVA}=0.0016$) for the targeted LC-MS-based characterisation of prostaglandins and unsaturated fatty acids in blue mussel post-larvae (Fig. 3).

Compound	Contribution	VIP
(±)9(10)-DiHOME	-1.37425	1.05501
11-HEPE	-2.36357	1.27140
13,14-dihydro-15-Keto-PGF2 α	0.02000	0.68116
13-HDHA	-2.62205	1.28919
15-HEPE	-1.13632	0.99026
15-keto-PGE2	-1.31368	1.02460
15-keto-PGF2 α	-2.34545	1.25178
16-HDHA	0.60088	0.85104
20-HDHA	0.23909	0.78353
8-HDHA	-2.32204	1.22525
8-HEPE	-1.75619	1.14781
9(S)-HOTrE	0.09783	0.75118
PGA2	0.489607	0.62523
PGF3 α	-0.02746	0.65959

¹H-NMR: 67 metabolites detected

Acetate	Homarine
Acetoacetate	Hypotaurine
Acetone	IMP
Acetylcarnitine	Inosine
Acetylcholine	Isoleucine
Alanine	Isopropanol
Alloisoleucine	Ketoleucine
alpha Aminobutyrate	Lactate
AMP	Leucine
Arginine	Lysine
Asparagine	Malonate
Aspartate	Maltose
beta-Alanine	Mannitol
Betaine	Methionine
Carnitine	myo-Inositol
Choline	Mytilitol
Citrate	Ornithine
Creatine	Phenylalanine
Cysteine	Phosphocholine
Dimethyl sulfone	Phosphocreatine
Dimethylglycine	Phosphoethanolamine
Ethanol	Proline
Formate	Propionate
Fumarate	Pyruvate
Glucose	Sarcosine
Glucose-6-phosphate	Serine
Glutamate	Glycerophosphocholine
Glutamine	Succinate
Glycine	Taurine
Guanidoacetate	Theophylline



LC-MSMS (ESI + & -): 84 metabolites annotated

(2R)-3-Hydroxyisovalerylcarnitine	Diethylene glycol*	Phenylalanine
.alpha.-L-Glu-L-Tyr	Diethylene glycol monoethyl ether*	Phosphocholine
1,11-Undecanedicarboxylic acid	Ethyl 3-hydroxybenzoate*	Phthalic anhydride*
1,2-Benzenedicarboxylic acid*	Glycerophosphocholine	Pipecolate
1,3-Dicyclohexylurea	Guanine	Propionylcarnitine
15-Deoxy-.DELTA.12,14-prostaglandin J2	Guanosine	p-tert-Butylcatechol
1-Aminocyclopropanecarboxylic acid	Guanosine monophosphate	Pyroglutamate
1-Myristoyl-sn-glycero-3-phosphocholine	Hexaethylene glycol*	Riboflavin
2-Phenylacetamide	Hexanoyl-L-carnitine	S-(5'-Adenosyl)-L-homocysteine
3-Cyclohexyl-1,1-dimethylurea	Hexapropylene glycol*	Sebateate
3-Indoleacrylic acid	Hypoxanthine	Stachydrine
4,5.alpha.-Dihydroneoethisterone	Indole-6-carboxaldehyde	Stearidonate
4-Ethoxybenzoic acid*	Inosine	Taurine
4-Nitrophenol*	Inosinic acid	Tetradecanedioate
4-Picoline	Isobutyryl-L-carnitine	Tetraethylene glycol*
5-Isoprostaglandin-F2.alpha.-VI	Isophorone*	Thymoquinone
5'-S-Methyl-5'-thioadenosine	L-.gamma.-Glutamyl-L-glutamic acid	Tri(3-chloropropyl) phosphate*
7-Methylguanidine	Lactate	Tributylamine*
Acetylcarnitine	Leucine	Trigonelline
Adenosine	Malate	Tryptophan
ADP	Methionine	Tyrosine
Alanine	Myristoleate	Uracil
AMP	Myristoyl-L-carnitine	Uridine
Aspartate	Nicotinate	Urocanate
Azelate	Ophthalmic acid	Xanthurenate
Benzanilide*	Palmitoylcarnitine	
Benzophenone*	Pantothenate	
Carnitine	Pentapropylene glycol*	
Citrate		
Cysteine-glutathione disulfide		
Diethyl phthalate*		

Fig. S3. List of the metabolites detected by ¹H-NMR and detected and annotated by LC-MSMS in the untargeted metabolomics analysis of blue mussel post-larvae. *Compounds excluded from the analysis as suspected contaminants based on data in the Human Metabolome Database (<https://hmdb.ca>)

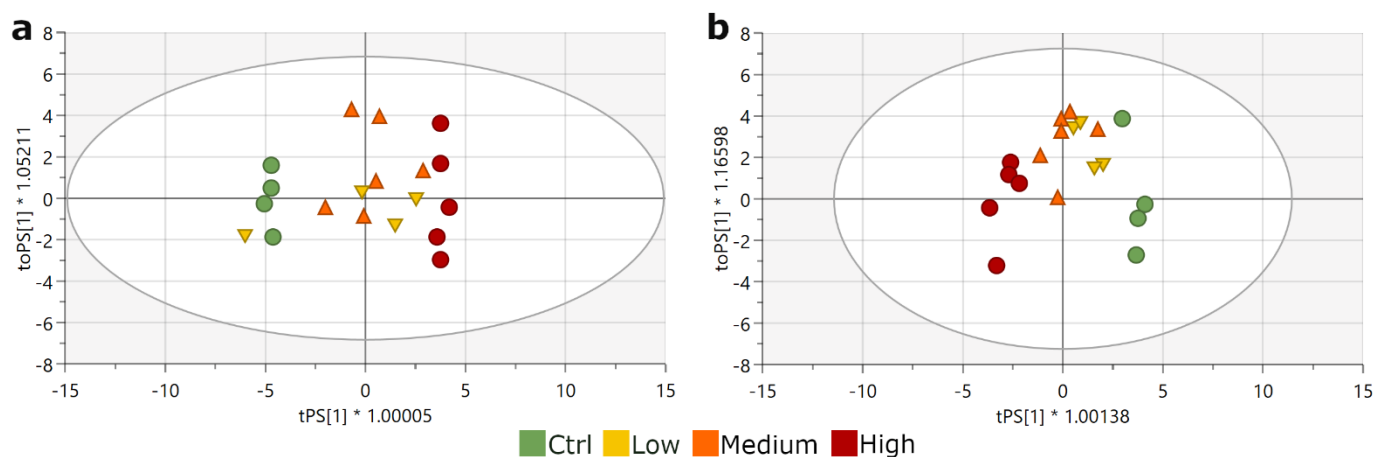


Fig. S4. a, Parsimonious OPLS-DA scores plot based upon the fitted model ($R^2Y=1$, $Q^2=0.99$, CV-ANOVA=0.0005, 36 features) on the untargeted NMR data from blue mussel post-larvae. Green circles: control, yellow inverted triangles: low, orange triangles: medium, and red boxes: high shipping noise. **b**, Parsimonious OPLS-DA scores plot based upon the fitted model ($R^2Y=0.98$, $Q^2=0.90$, CV-ANOVA=0.0275, 28 features) on the untargeted LC-HRMS data. Green circles: control, yellow inverted triangles: low, orange triangles: medium, and red boxes: high shipping noise.

Table S4. Contribution and importance of the variables in the projection (VIP) of the metabolites included in the multi-block OPLS-DA model ($R^2Y=1.00$, $Q^2=0.98$, $CV\text{-ANOVA}=0.0010$) for the untargeted LC-MS (green) and NMR (yellow) -based metabolomics of blue mussel post-larvae (Fig. 4).

Metabolite (chemical shift)	Contribution	VIP
15-Deoxy-Δ12,14-prostaglandin J2	-1.91282	1.2142
Acetylcarnitine	-1.03669	0.8516
Acetylcholine (3.227)	1.98841	1.0722
Adenosine	-2.07545	1.2191
Alanine (3.769)	-1.41936	0.9114
Alanine (3.780)	-1.22053	0.8513
Arginine (3.775)	-1.54783	0.9528
Asparagine (2.851)	0.714892	0.6348
Aspartate	2.14305	1.2373
Aspartate (3.888)	1.62194	1.0120
β -Alanine (2.564)	-1.99612	1.0699
β -Alanine (3.170)	-1.77388	1.0225
β -Alanine (3.182)	-1.8582	1.0411
β -Alanine (3.191)	-1.8117	1.0286
Dimethyl sulfone (3.151)	1.72833	0.9958
γ -Glutamyl-glutamic acid	-1.42953	1.0990
Glutamate (3.753)	-1.85861	1.0375
Glutamate (3.759)	-1.9704	1.0664
Glutamate (3.772)	-1.68471	0.9953
Glutamine (3.765)	-1.61215	0.9787
Glutamine (3.786)	-1.15392	0.8363
Glycine (3.563)	1.04622	0.8467
Hypoxanthine	-1.47309	1.1620
Inosine (4.436)	0.761747	0.7055
Isobutyryl-carnitine	1.35022	0.9760
Leucine	-2.14092	1.2338
Methionine	-1.66535	1.1038
Methionine (2.648)	-0.45398	0.6326
Palmitoylcarnitine	-0.79373	0.8246
Phenylalanine	-1.41777	1.0852
Phosphocholine (3.220)	1.46923	0.9566
Pipecolic acid	2.17632	1.2433
Riboflavin	-1.81308	1.1789
Stearidonic acid	-1.10188	0.9089
Unknown 1 (3.747)	-1.29557	0.8690
Unknown 2 (1.884)	1.88602	1.0524
Unknown 3 (1.520)	-0.704	0.6964
Uridine	0.312618	0.8998

Table S5. Targeted LC-MS-based quantification of amino acids and energy metabolism metabolites in blue mussel post-larvae. The significance of the differences in concentrations of the metabolites between noise levels was tested by Permanova (P-value < 0.05). Significant differences of concentration are indicated by letters.

Metabolic pathway	Metabolite	Control	Low	Medium	High
Aerobic (mitochondria - Krebs and urea cycle)	α-Ketoglutarate	0.9±0.2	3.4±1.3	4.5±1.8	3.1±0.3
	Cis-aconitate	1.96'10 ⁻² ±0.01	6.85'10 ⁻² ±0.03	9.88'10 ⁻² ±0.02	2.86'10 ⁻² ±0.02
	Citrate	18.6±2.1	30.9±5.6	29.1±3.1	113.7±59.6
	Succinate	260.4±37.4	226.6±61.0	277.7±23.8	443.2±95.0
	Fumarate	17.5±2.1	26.7±8.7	24.6±5.2	24.0±10.0
	Malate	283.3±39.8	368.4±103.7	347.3±74.6	636.2±218.2
	Oxaloacetate	16.9±4.9^b	47.7±10.2^{ab}	23.5±7.0^{ab}	41.4±24.3^a
	Glutamate	2764.7±93.5	1710.5±167.1	2099.3±344.5	3932.6±1415.7
	Glutamine	1282.2±50.1	1202.7±35.8	1180.0±66.2	1014.5±315.2
	Arginine	1397.1±80.6	1229.3±147.7	1309.6±65.5	1296.6±396.9
Anaerobic (lactic fermentation - glycolysis)	Strombine	2792.6±96.0	1741.2±168.6	2141.1±347.1	3862.3±1345.3
	Octopine	143.6±17.5	137.4±38.3	116.8±14.2	104.8±14.9
	Lactate	104.5±5.8	125.6±28.7	129.5±10.5	126.2±24.3
Molecule and coenzymes related to energy transfer	AMP	291.7±26.5	194.0±44.7	228.8±35.9	1174.8±661.6
	ADP	2.7±0.6	30.3±27.5	10.4±3.6	4.7±2.7
	ATP	14.3±2.9	16.6±3.2	16.8±2.0	30.8±19.2
	NAD	25.6±3.1	15.1±8.3	12.2±5.5	30.6±24.8
	NADH	11.3±2.8	7.4±1.7	10.4±2.7	14.7±10.9
	NADP	4.8±1.4	9.2±4.1	7.3±1.7	3.9±2.8
	NADPH	47.4±9.5	48.7±7.5	59.4±7.5	159.6±101.9
	FAD	0.1±0.02	0.1±0.05	0.1±0.05	0.3±0.5
	Glucose	115.1±4.9	137.3±23.8	121.4±5.7	129.2±10.3
	Glucose-6-phosphate	96.0±16.7	104.6±28.7	124.4±11.6	1080.1±716.9
	Pyruvate	39.7±2.3	22.7±4.6	34.0±6.3	20.5±7.8
	Phosphoenol pyruvate	2.1±0.4	2.7±0.9	2.2±0.4	2.2±0.6
	Acetyl-Coa	0.8±0.1^b	1.1±0.2^{ab}	0.9±0.2^{ab}	1.9±0.8^a
D-Fructose-1,6-biphosphate trisodium	23.6±2.4	24.1±3.2	41.4±6.8	24.2±11.9	
Essential amino acids	Histidine	441.3±10.4^a	304.6±22.0^{ab}	241.4±16.5^b	1167.9±514.4^{ab}
	Methionine	32.1±2.1^a	26.4±2.4^{ab}	23.0±1.4^b	24.4±3.8^{ab}
	Threonine	469.7±25.6	451.8±8.7	465.0±17.2	582.2±163.5
	Tryptophan	79.0±4.2	82.1±5.3	68.2±4.1	73.9±9.5
	Phenylalanine	442.9±20.1	456.4±24.5	432.3±28.1	480.1±90.2
	Valine	427.2±19.6	459.2±19.4	465.6±37.2	545.2±66.7
	Leucine	384.2±21.4	413.0±13.3	405.5±28.8	545.9±19.8
	Isoleucine	144.9±6.6	145.6±4.3	139.0±7.8	158.6±24.4
	Lysine	123.2±6.6	119.1±16.9	103.5±6.6	115.2±38.3
Non-essential amino acids	Proline	765.8±60.4^a	484.8±15.1^b	525.8±70.3^b	330.0±89.6^b
	Hydroxyproline	40.2±3.4	38.9±2.6	41.0±3.7	52.2±15.2
	Cystine	3.3±0.5	6.1±1.1	6.0±0.7	88.7±59.7
	Tyrosine	559.3±21.5^b	545.5±14^b	596.2±31.7^{ab}	730.8±141.9^a
	Alanine	3560.6±181.0	2889.2±190.0	2812.3±136.8	3299.1±679.6
	Serine	1000.6±56.2	919.6±42.4	1015.9±29.3	1037.1±34.1
	Glycine	8634.4±362.8	7579.1±849.1	7490.3±670.9	7118.2±1664.6
	Aspartate	1832.0±85.3	1606.6±201.1	1769.4±163.3	1844.8±602.4
	α-Aminobutyric acid	2580.6±250.0	1630.1±118.2	2006.1±205.5	4175.7±1285.1
	α-Amino adipic acid	60.9±4.6	35.2±4.3	41.7±4.0	185.0±84.6
	β-Aminoisobutyric acid	189.2±14.9	164.2±24.6	165.4±13	157.8±23.5
	Betaine	13286.7±986.2	15319.0±1354.6	13971.5±1123.1	16407.4±10384.9
	Ratio	Glycine/Succinate	37.2±6.0	40.4±10.7	25.5±4.4
AEC [†]		0.05±0.00	0.13±0.10	0.09±0.00	0.10±0.10
BCAAs [‡]		956.3±47.0	1017.8±32.8	1010.1±72.6	1249.8±288.4
NADH/NAD ⁺		0.6±0.2	1.3±0.7	1.4±0.5	8.2±5.8

[†]Adenylic Energetic Charge. Stress index defined as: (ATP + 0,5ADP)/(ATP + ADP + AMP)

[‡]Branched-chain amino acid. Indicator of muscle energy: valine + leucine + isoleucine

Table S6. Contribution and importance of the variables in the projection (VIP) of the metabolites included in the OPLS-DA model ($R^2Y_{cum}=1.00$, $Q^2_{cum}=0.99$, CV-ANOVA=0.0245) for the targeted LC-MS-based characterisation of amino acids and energy metabolism in blue mussel post-larvae (Fig. 4)

Metabolite	Contribution	VIP
Acetyl-Coa	1.68002	1.08603
ADP	1.23701	1.01615
Aketoglutarate	2.64558	1.25994
ATP	0.869137	0.938782
Glucose	0.913422	0.957866
Glutamate	-2.01153	1.13567
Glutamine	-1.06618	0.928844
Glycine	-1.01697	0.956994
Lactate	0.465301	0.861751
Leucine	1.10796	0.939639
Methionine	-1.30631	0.990473
NADPH	0.937975	0.966666
Octopine	-0.622776	0.871872
Oxaloacetate	1.95708	1.08207
Phosphoenol pyruvate	0.109994	0.733108
Proline	-1.91747	1.09706
Pyruvate	-1.22877	1.0199
Strombine	-1.97715	1.12948
Threonine	0.779409	0.80869
Tyrosine	1.59111	1.0074
Valine	1.78067	1.06564

TEXT S1. SPECTROSCOPIC METHODS

S1.1. Untargeted ¹H-NMR-based metabolomics

NMR measurements were performed at 298K. Spectra were acquired using an NOESY pulse sequence with a repetition delay of 10 s and mixing time of 50 ms. Water suppression was achieved by presaturation during the repetition delay and mixing time. ¹H spectra were collected with 1,024 transients, 64 k data points and a spectral width of 12 ppm. Spectra were processed using NMRProcFlow tools. Free induction decays (FIDs) were zero-filled to 128k data points, a line-broadening factor of 0.3 Hz was applied prior to Fourier transform, and the 3-trimethylsilylpropionic acid referenced to 0 ppm. Larval extracts spectra were then bucketed manually and integrated. Signals from water, methanol, and all the buckets with a signal-to-noise ratio inferior to 3 were excluded. Data were normalized by the total sum of all of the spectral features and the generated data table was used for multivariate statistical analyses. Identification of metabolites was performed using Chenomx software (Edmonton, Canada), HMDB <https://hmdb.ca/>¹. Annotations of the spectra were further confirmed by 2D ¹H-NMR COSY and TOCSY experiments performed on a representative sample.

S1.2. Untargeted LC-HRMS-based metabolomics

Liquid chromatography–high resolution tandem mass spectrometry analyses were performed on a Shimadzu Nexera UHPLC coupled to a quadrupole time-of-flight system (TripleTOF® 5600+, Sciex, Concord, ON, Canada). Metabolite separation was conducted on a mixed-mode reverse-phase column (Imtakt USA, Scherzo SM-C18, 150x3 mm, 3 μm), using gradient elution with mobile phases of water and acetonitrile (ACN), both containing 0.1% formic acid with a 0.3 ml/min flow rate. The gradient started at 3% B (held for 2 min), then increased linearly reaching 65% at 15 min, then rapidly up to 95% at 15.5 min, held to 18 min, then decreased to 3% for 7 min of column re-equilibration, with a total run time of 25 min. Electrospray ionization (using a Duospray source) was used in positive and negative mode, with the following parameters: ionization potential +5000 or – 4500 V, source temperature 450 °C, curtain gas of 35 psi, drying and nebulization gas flow rate 50 psi. TOF-MS data were acquired from *m/z* 80-980 with a cycle time of 1.1 s and a collision-offset voltage (CE) of 30 ± 10V, then MS/MS was conducted on precursors between *m/z* 80-800, in information-dependent (IDA) mode choosing the 8 most intense ions, with dynamic background subtraction. MS/MS spectra were acquired in the range of *m/z* 40-800.

Peak finding was conducted using Markerview™ 1.3.1 (Sciex, Concord, ON, Canada), to generate a peak list of features to input into Sciex OS-Q 2.0.1 (Sciex, Concord, ON, Canada) for further identification of putative metabolites using MS/MS spectral matching via library searching on with NIST2017 MS/MS spectral library (with 13808 compounds) and Sciex “All in one” accurate mass metabolite library (650 metabolites), as well as an in-house spectral library containing 194 spectra from standard metabolites run under identical MS/MS conditions. Features with a library score ≥85 and an accurate mass measurement for protonated or deprotonated precursors <10 ppm were kept for further processing. Peak integrations were verified for each putatively identified metabolite using Sciex OS-Q™.

S1.3. Targeted LC-HRMS/MS based quantification of amino acids and metabolites from the energy metabolism and oxylipins

1. Oxylipins analysis

Oxylipins analysis was performed with an HPLC 1260 Infinity II device coupled to a 6546 QTOF (Agilent Technologies) in negative ionization mode equipped with an Agilent 1290 Infinity Flexible Cube. Oxylipins extracts were separated using an InfinityLab Poroshell HPH C-18, 2.1 x 100 mm 1.9 μm (Agilent) and a Gemini C6-Phenyl guard column as on-line SPE (4 x 2.0 mm, SecurityGuard, Phenomenex) with a column temperature maintained at 40°C.

One milliliter was injected on the small trapping column (Phenyl Hexyl 4 x 2.0 mm (SecurityGuard, Phenomenex)) with a mobile phase of 90/10 water/methanol (v/v) with 20 mM ammonium formate at pH 3 with a flow rate of 1 mL/min provide by an isocratic pump. A 3-second in-flush port for needle wash (isopropanol) was used. Extract trapped on SPE was washed with the isocratic mobile phase during 5 min and eluent was sent to the waste. Flow rate was reduced 5-5.01 min at 0.20 μL and maintained from 5.01 to 6 min. After 6 min, the Flexible Cube connected the SPE to the analytical column (InfinityLab Poroshell HPH C-18, 2.1 x 100 mm 1.9 μm (Agilent). For the analytical column, mobile phase (A) consisted of water/methanol (90:10, v/v) with 0.01% ammonium hydroxide, and mobile phase (B) of methanol/isopropanol (65:35, v/v) with 0.01% ammonium hydroxide. A gradient elution was applied to separate analytes. The gradient elution used was maintained to 0% B 0-10 min, increased to 40% B from 10 to 36 min, maintained at 40% B 36-40 min increased to 90% B 40-50 min, maintained at 100% B 50-54 min and return to initial conditions 54-56 min, with a flow rate at 0.2 mL/min. Total run was 60 min following by a 4 min post-run. The following parameters were used for the Flexibe Cube (**Figure S5**), on-line SPE mobile phase flux according to the Flexible Cube timetable (**Table S7**) and MS acquisition parameters (**Table S8**).

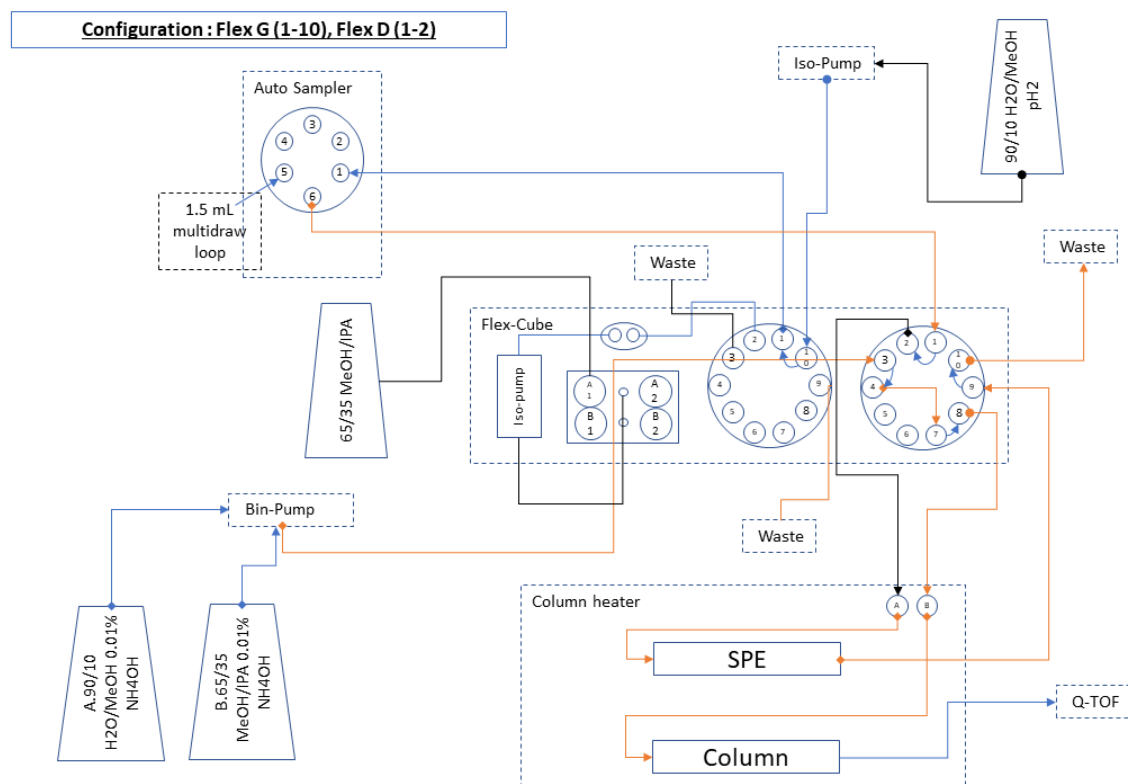


Figure S5. Diagram illustrative of the LC-HRMS/MS setup

Table S7. Flexible Cube timetable

Time (min)	Function	Parameter
0.00	Left valve change position	Position 1 (Port 1 -> 10)
0.00	Right valve change position	Position 2 (Port 1 -> 2)
6.00	Right valve change position	Position 1 (Port 1 -> 10)
7.00	Left valve change position	Position 2 (Port 1 -> 2)
7.01	Pump volume	Pump 2.5 mL, Flow: 1 mL/min, Channel A: A1, Channel B: Method setting
58.00	Left valve change position	Position 1 (Port 1 -> 10)
58.00	Right valve change position	Position 2 (Port 1 -> 2)

Table S8. Mass spectrometry acquisition parameters

MS source	Dual AJS ESI			
Acquisition mode	Negative			
Gas Temperature	200°C			
Gas flow	10 L/min			
Nebulizer	50 psi			
Sheath Gas Temp	300°C			
Sheath Gas Flow	12 L/min			
VCap	3000 V			
Nozzle Voltage	1000 V			
Fragmentor	150 V			
Skimmer	65 V			
Octopole RF	750 V			
Reference Mass	<i>m/z</i> 119.03632			
MS and MS/MS Range	MS: 100-500 <i>m/z</i> MS/MS: 50-400 <i>m/z</i>			
Min MS and MS/MS Scan Rate	MS: 4.00 spectra/s (250 ms/spectrum) MS/MS: 6.67 spectra/s (149.9 ms/spectrum)			
Quadrupole Resolved All Ions (Q-RAI) Mass Table	Start Mass	End Mass	Window Width	Collision Energy
	1 250	325	75	5
	2 250	325	75	15
	3 250	325	75	25
	4 325	375	50	5
	5 325	375	50	15
	6 325	375	50	25
Threshold for MS and MS/MS	MS: 200 counts and 0,010% MS/MS: 5 counts and 0,010%			

2. Amino acids, energy metabolism-related metabolite analysis

Metabolites were separated and quantified in multiple reaction monitoring using an HPLC 1260 Infinity II device coupled to a 6420 Triple Quad mass spectrometer (Agilent Technologies) in positive and negative ionization mode. Ten microliters of the sample were injected, and the chromatography separation was performed with a InfinityLab Poroshell 120 HILIC-Z, 2.7 μm . 10 x 2.1 mm column. Mobile phase, gradients and mass spectrometer parameters (**Table S9**) differ according to the detection mode. The precursor ion for the positive and negative ionisation modes are listed in **Tables S10** and **S11**, respectively. This method makes it possible to detect 30 metabolites with the positive analysis and 20 metabolites resulting from the negative analysis, see Table S4.

Table S9. LC-HRMS/MS setup and parameters

	Positive ionisation mode		Negative ionization mode	
Column	InfinityLab Poroshell 120 HILIC-Z, 2.7 μm . 10 x 2.1 mm		InfinityLab Poroshell 120 HILIC-Z, 2.7 μm . 10 x 2.1 mm	
Guard column	InfinityLab Poroshell 120 HILIC-Z, 2.7 μm . 2.1 x 5 mm		InfinityLab Poroshell 120 HILIC-Z, 2.7 μm . 2.1 x 5 mm	
Column temperature	30°C		30°C	
Injection volume	10 μL		10 μL	
Autosampler	4°C		4°C	
Needle wash	5s Flush Port (10/90 ACN/H ₂ O)		3s Flush Port (10/90 ACN/H ₂ O)	
Mobile phase	A) 20 mM Ammonium Formiate pH 3, H ₂ O-MS B) 20 mM Ammonium Formiate pH 3, 90:10 ACN-MS: H ₂ O-MS		A) 10 mM Ammonium Acetate, 5 μM deactivator pH 9, H ₂ O-MS, 0.2 mM NH ₄ F B) 10 mM Ammonium Acetate, 5 μM deactivator pH 9, 90:10 ACN-MS: H ₂ O-MS, 0.2 mM NH ₄ F	
Flow rate	500 $\mu\text{L}/\text{min}$		250 $\mu\text{L}/\text{min}$	
Gradient program	Time (min)	%B	Time (min)	%B
	0	100	0	90
	14	70	2	90
	15.5	100	12	60
	17	100	15	60
			16	90
			24	90
Run time	17 min		24 min	
Post time	4 min		0 min	
MS source	ESI		ESI	
Gas Temp (°C)	340°C		0-4 min: 200°C 4-16 min: 340°C	
Gas Flow	13 L/min		13 L/min	
Nebulizer	30 psi		30 psi	
Capillary	3500 V		3500 V	
Scan type	MRM		MRM	
Cycle Time (Dwell)	25 ms		0-4 min: 100 ms 4-16 min: 15 ms	
MS1 and MS2 resolution	Unit		Unit	
CAV	7		7	

Table S10. Precursor ion, product ion, RT and QQQ parameters for each compound in positive mode.

Compound	Precursor Ion	Product Ion	RT (min)	Frag	CE
α -aminoadipic acid	162.1	98.0	9.055	80	12
α -aminoisobutyric acid	104.1	57.0	7.640	60	12
Alanine	90.1	44.2	7.887	40	8
AMP	348.0	136.1	9.718	128	12
Arginine	175.1	70.2	11.658	100	24
Aspartate	134.0	74.0	10.528	60	8
β -aminoisobutyric acid	104.1	86.1	7.688	60	4
Betaine	118.1	58.0	5.119	128	28
Cystine	241.0	74.0	12.525	80	24
FAD	786.3	348.0	10.449	124	12
Glutamate	148.1	84.0	9.669	80	12
Glutamine	147.1	84.0	8.896	60	16
Glycine	76.1	30.2	8.617	40	4
Histidine	156.1	110.0	11.074	80	12
Hydroxyproline	132.1	86.2	8.055	80	12
Isoleucine	132.1	86.2	5.248	60	4
Leucine	132.1	86.2	4.801	60	4
Lysine	147.1	84.0	12.389	80	16
Methionine	150.1	133.0	5.725	80	4
NAD	664.0	428.1	12.090	128	24
Phenylalanine	166.1	120.2	4.270	80	8
Proline	116.1	70.0	6.799	80	12
Sarcosine	89.9	44.0	8.082	40	8
Serine	106.0	60.0	8.907	60	8
Strombine	148.0	102.0	9.669	63	6
Threonine	120.1	74.1	8.241	60	4
Tryptophan	205.1	188.3	4.613	80	0
Tyrosine	182.1	165.2	6.430	60	4
Valine-d ₈	126.0	80.0	6.687	60	4
Valine	118.1	72.0	6.649	60	4

Table S11. Precursor ion, product ion, RT and QQQ parameters for each compound in negative mode.

Compound Name	Precursor Ion	Product Ion	RT (min)	Frag	CE	Type	Mode
Acetyl CoA	403.6	403.6	11.649	50	0	Quantifier	Negative
Acetyl CoA	403.6	79.0	11.649	50	40	Qualifier	Negative
ADP	426.0	426.0	12.126	75	0	Quantifier	Negative
ADP	426.0	79.0	12.126	75	48	Qualifier	Negative
ATP	506.0	506.0	12.618	150	0	Quantifier	Negative
ATP	506.0	159.0	12.618	150	44	Qualifier	Negative
Cis-Aconitate	173.0	173.0	11.157	60	0	Quantifier	Negative
Cis-Aconitate	173.0	129.0	11.157	60	0	Qualifier	Negative
Citrate	191.0	191.0	12.614	75	0	Quantifier	Negative
Citrate	191.0	111.0	12.614	75	8	Qualifier	Negative
D-Fructose-1,6-biphosphate	339.0	339.0	14.152	100	0	Quantifier	Negative
D-Fructose-1,6-biphosphate	339.0	97.0	14.152	100	20	Qualifier	Negative
Fumarate	115.0	115.0	10.639	75	0	Quantifier	Negative
Fumarate	115.0	71.0	10.639	75	0	Qualifier	Negative
Glucose	179.0	89.0	2.974	60	4	Quantifier	Negative
Glucose-6-phosphate	259.0	259.0	12.590	75	0	Quantifier	Negative
Glucose-6-phosphate	259.0	199.0	12.590	75	4	Qualifier	Negative
Lactate	89.0	89.0	2.973	50	0	Quantifier	Negative
Lactate	89.0	43.0	2.973	50	8	Qualifier	Negative
Malate	133.0	133.0	10.806	75	0	Quantifier	Negative
Malate	133.0	115.0	10.806	75	4	Qualifier	Negative
NADH	664.1	664.1	10.346	160	0	Quantifier	Negative
NADH	664.1	408.0	10.346	160	32	Qualifier	Negative
NADP	742.1	742.1	13.780	75	0	Qualifier	Negative
NADP	742.1	620.0	13.780	75	10	Quantifier	Negative
NADPH	744.1	744.1	13.198	75	0	Quantifier	Negative
NADPH	744.1	408.0	13.198	75	30	Qualifier	Negative
Octopine	247.0	247.0	11.974	4	0	Quantifier	Positive
Octopine	247.0	70.0	11.974	4	35	Qualifier	Positive
Oxaloacetate	131.0	87.0	12.198	75	0	Quantifier	Negative
Phosphoenol pyruvate	166.9	78.8	12.933	75	4	Quantifier	Negative
Pyruvate	87.0	87.0	1.962	60	0	Quantifier	Negative
Pyruvate	87.0	43.0	1.962	60	0	Qualifier	Negative
Pyruvate d ₃	90.0	90.0	1.964	50	0	Quantifier	Negative
Pyruvate d ₃	90.0	46.0	1.964	50	0	Qualifier	Negative
Succinate	117.0	117.0	10.898	75	0	Quantifier	Negative
Succinate	117.0	99.0	10.898	75	8	Qualifier	Negative
Succinyl CoA	866.6	866.6	13.318	100	0	Qualifier	Negative
Succinyl CoA	866.6	408.0	13.318	100	40	Quantifier	Negative
α -ketoglutarate	145.1	145.1	9.339	60	0	Quantifier	Negative
α -ketoglutarate	145.1	101.0	9.339	60	0	Qualifier	Negative